Physica D 280–281 (2014) 95–108

Contents lists available at ScienceDirect

Physica D

journal homepage: www.elsevier.com/locate/physd

Regularized model of post-touchdown configurations in electrostatic MEMS: Equilibrium analysis

A.E. Lindsay [a,*], J. Lega [b], K.B. Glasner [b]

[a] Department of Applied and Computational Mathematics and Statistics, University of Notre Dame, South Bend, IN, 46556, USA
[b] Department of Mathematics, University of Arizona, Tucson, AZ, 85721, USA

HIGHLIGHTS

- We propose a regularized model for electrostatic MEMS.
- Solutions are bounded and undergo additional dynamics after touchdown.
- Convergence to a new branch of equilibria, which is absent in the non regularized equations.
- The regularization equations have bistable equilibrium structure.

ARTICLE INFO

Article history:
Received 1 August 2013
Received in revised form
20 March 2014
Accepted 20 April 2014
Available online 30 April 2014
Communicated by K. Promislow

Keywords:
Singular perturbation techniques
Nano-technology
Regularization
Blow up
Higher order partial differential equations

ABSTRACT

In canonical models of Micro-Electro Mechanical Systems (MEMS), an event called touchdown whereby the electrical components of the device come into contact, is characterized by a blow up in the governing equations and a non-physical divergence of the electric field. In the present work, we propose novel regularized governing equations whose solutions remain finite at touchdown and exhibit additional dynamics beyond this initial event before eventually relaxing to new stable equilibria. We employ techniques from variational calculus, dynamical systems and singular perturbation theory to obtain a detailed understanding of the properties and equilibrium solutions of the regularized family of equations.

1. Introduction and statement of main results

Micro-Electro Mechanical Systems (MEMS) are a large collection of miniaturized integrated circuits and moving mechanical components that can be fabricated together to perform a multitude of tasks. MEMS practitioners aim to manipulate the interaction between electrostatic forces and elastic surfaces to design a variety of complex devices with applications in drug-delivery [1,2], micro pumps [3], optics [4], micro-scale actuators [5]. In such interactions, the elastic structures of the MEMS device may be overwhelmed if the magnitude of the electrostatic forces acting on them exceeds a critical threshold. Such a failure is manifested by an instability, known as the *pull-in instability*.

In a capacitor type MEMS device, an elastic membrane is held fixed along its boundary above a rigid substrate. When an electric potential V is applied between these surfaces, the upper elastic surface deflects downwards towards the substrate. If V is small enough, the deflection will reach an equilibrium, however, if V exceeds the *pull-in voltage* V^*, no equilibrium configuration is attainable and the top plate will touch down on the substrate. Fig. 1 contains a schematic representation of the device.

Touchdown is a very rapid event whereby large quantities of energy are focused on small spatial regions of the MEMS device over short time scales. Consequently this process develops large forces at specific areas which can either be useful to the operation of the device or be destructive. In many mathematical models of MEMS, touchdown is described by finite time quenching, e.g. blow-up of solution derivative and energy. Accordingly, many important operational aspects of MEMS, such as the time and location of touchdown, can be investigated by studying this quenching event.

However, a loss of existence to model solutions results in no information regarding configurations of MEMS after a primary

* Corresponding author. Tel.: +1 5746313511.
E-mail addresses: a.lindsay@nd.edu (A.E. Lindsay), lega@math.arizona.edu (J. Lega), kglasner@math.arizona.edu (K.B. Glasner).

http://dx.doi.org/10.1016/j.physd.2014.04.007
0167-2789/

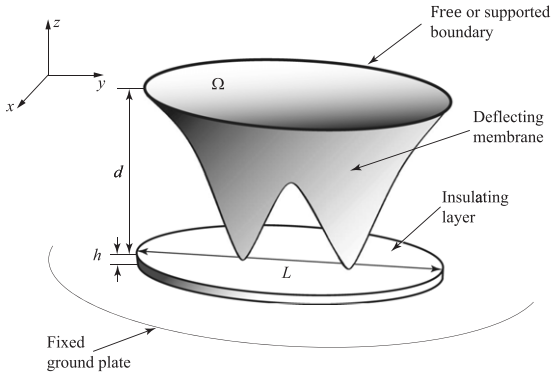

Fig. 1. Schematic diagram of a MEMS capacitor with insulating layer of thickness h.

touchdown event. This paper presents an initial attempt to describe behavior of MEMS after touchdown. To this end, we derive the second order equation

$$u_t = \Delta u - \frac{\lambda}{(1+u)^2} + \frac{\lambda\varepsilon^{m-2}}{(1+u)^m}, \quad x \in \Omega; \qquad u = 0, \quad x \in \partial\Omega, \tag{1.1a}$$

which models the dimensionless deflection $u(x,t)$ as that of a membrane, and the fourth order problem

$$u_t = -\Delta^2 u - \frac{\lambda}{(1+u)^2} + \frac{\lambda\varepsilon^{m-2}}{(1+u)^m}, \quad x \in \Omega; \qquad u = \partial_n u = 0, \quad x \in \partial\Omega, \tag{1.1b}$$

which is a beam description of the deflecting surface. The modeling literature on MEMS has involved the second (cf. [6–11]) and fourth order (cf. [12–16]) descriptions of the elastic nature of the deflecting surface and so we aim to investigate the effects of regularization on both. In both cases, Ω is a bounded region of $\mathbb{R}^n$ and $\lambda \propto V^2$ is a parameter quantifying the relative importance of electrostatic to elastic forces. The physically relevant dimensions are $n = 1, 2$. The small parameter ε in (1.1) mimics the effect of a small insulating layer placed on top of the substrate to prevent a short circuit of the device as the gap spacing $1 + u$, $u < 0$, locally shrinks to zero. The regularizing term $\lambda\varepsilon^{m-2}(1+u)^{-m}$ for $m > 2$ can also account for a variety of physical effects which become important when $u \approx -1$. For example $m = 4$ accounts for the Casimir effect (with sign of regularizing term reversed) while $m = 3$ models Van der Waals forces [17,18]. A recent mathematical study has analyzed the existence and stability of equilibria to (1.1a) in the case $m = 4$ [19]. Similar quenching events and their regularizations have been investigated in studies of thin film dynamics on solid substrates [20–22].

For the case $\varepsilon = 0$, Eqs. (1.1) reduce to canonical models originally introduced by Pelesko (cf. [23,10]), the salient properties of which are now well known. Of particular importance amongst the many results, is the existence of a pull-in voltage λ^* such that if $\lambda < \lambda^*$, then $u(x,t)$ approaches a unique and stable equilibrium as $t \to \infty$, while for $\lambda > \lambda^*$ no equilibrium solutions are possible and $u(x,t)$ reaches -1 in some finite time, t_c [24,8,25]. In the 1D setting, the equilibrium structure consists of one stable and one unstable branch that meet at λ^* (cf. dashed curve of Fig. 4). In the case where $\lambda > \lambda^*$, there have been many studies centered on describing the local properties of the device near touchdown. For example, in the second order equation,

$$u_t = \Delta u - \frac{\lambda}{(1+u)^2}, \quad x \in \Omega, \tag{1.2}$$

a detailed analysis [8,26,20,27] of solutions near touchdown reveals the local behavior

$$u \to -1 + [3\lambda(t_c - t)]^{1/3} \times \left(1 - \frac{1}{2|\log(t_c - t)|} + \frac{(x - x_c)^2}{4(t_c - t)|\log(t_c - t)|} + \cdots\right), \tag{1.3}$$

in the vicinity of the touchdown point x_c, for $t \to t_c^-$. Detailed scaling laws for t_c in the limits $\lambda \to \infty$ and $\lambda - \lambda^* \to 0^+$ have also been established in [6,7]. In the fourth order problem,

$$u_t = -\Delta^2 u - \frac{\lambda}{(1+u)^2}, \quad x \in \Omega, \tag{1.4}$$

less is known about equilibrium configurations and about the dynamics of touchdown when equilibrium solutions do not exist. In the special cases where Ω is the unit strip $[-1, 1]$ or the unit disc $\{x \in \mathbb{R}^2 \mid |x| \le 1\}$, the existence of the pull-in voltage λ^* was shown in [28,29]. It was shown in [16] that there are at least two radially symmetric solutions for each $\lambda < \lambda^*$. Similar results were obtained in [15] for the case where pinned boundary conditions $u = \Delta u = 0$ were used. For $\lambda > \lambda^*$ and for Ω the unit strip $[-1, 1]$ or the unit disc $\{x \in \mathbb{R}^2 \mid |x| \le 1\}$, it was shown in [13] that the device touches down in finite time t_c. A detailed numerical and asymptotic study established the local behavior

$$u(x,t) \to -1 + (t_c - t)^{1/3} v(y), \quad y = \frac{x - x_c}{(t_c - t)^{\frac{1}{4}}}\lambda^{1/4}, \quad t \to t_c^-, \tag{1.5}$$

where $v(y)$ is a self-similar profile satisfying an associated ordinary differential equation. In addition to the local behavior of solutions as $t \to t_c^-$, the fourth order problems (1.4) have additional interesting dynamical features whereby touchdown can occur simultaneously at multiple points of the domain. In one dimension [13], the singularities can form at two distinct points separated about the origin. In two dimensions [12], the multiplicity of singularities can be greater with the exact quenching set depending delicately on the geometry of the boundary and the parameter λ. This multiple singularity phenomenon is ubiquitous in semi-linear parabolic fourth order equations with positive sources [30].

The rich dynamical behavior associated with the touchdown event raises the interesting question of how one can make sense of solutions to (1.2) and (1.4), and understand the behavior of MEMS after touchdown. The finite time singularities exhibited by (1.2) and (1.4) result in the gap spacing $1 + u$ becoming arbitrarily small as $t \to t_c^-$ for λ sufficiently large. Consequently, a physically unreasonable situation occurs—the electric field generated between the plates becomes arbitrarily large as $t \to t_c^-$. The focus of this paper is first to regularize the singularity in the electric field at touchdown, thereby rendering it large but finite thereafter, and second to describe the post-touchdown equilibrium configurations of the resulting model. We obtain suitable regularized equations in Section 2 and analyze their properties in Section 3. First, we show in Section 3.1 that the regularized equations are globally well-posed. The variational nature of these equations then leads us to consider equilibrium solutions. Numerical simulations shown in Section 3.2 indicate that the regularized equations we propose undergo additional dynamics beyond the initial touchdown event (see for instance Fig. 3) and converge towards a new branch of equilibrium solutions. We show the corresponding bifurcation diagrams in Section 3.3 and explain how the new branch of solutions appears in Section 3.4. We then describe the properties of post-touchdown equilibrium configurations in terms of matched asymptotic expansions in Section 4. We summarize our results in Section 5 and discuss implications of the present work, in particular regarding the bistable nature of the proposed regularized equations.

2. Regularized governing equations

In this section we develop a new model for the operation of a MEMS device with a small insulating layer resting on the substrate, whose purpose is to physically prevent the occurrence of a short circuit. Based on this principle, the model features an obstacle type regularization of touchdown, in the form of a perturbed electrostatic potential with a repulsive term that mimics the obstacle.

In dimensional form, the model requires that the vertical (i.e. parallel to the z-direction) deflection $u(x, y, t)$ of a plate occupying a region $\Omega \subset \mathbb{R}^2$ with boundary $\partial\Omega$, satisfies [23]

$$\rho\, h_0 \frac{\partial^2 u}{\partial t^2} + a\frac{\partial u}{\partial t} + EI\,\Delta_\perp^2 u - T\,\Delta_\perp u = -\frac{\epsilon_0}{2}\,|\nabla\phi|^2_{z=u} \quad x \in \Omega; \tag{2.1a}$$

$$\nabla\cdot(\sigma\nabla\phi) = 0 \qquad -(d+h) \le z \le u(x, y, t), \tag{2.1b}$$

where $\perp$ indicates differentiation with respect to the x and y directions, and the permittivity σ satisfies

$$\sigma = \begin{cases} \sigma_0, & -d \le z \le u(x, y, t) \\ \sigma_1, & -(d+h) \le z \le -d. \end{cases} \tag{2.1c}$$

In Eq. (2.1), ρ, h_0, EI, and T are the density per unit length, thickness, flexural rigidity and tensile load of the plate. The term u_{tt} is the acceleration of the beam while u_t, $\Delta_\perp^2 u$, $\Delta_\perp u$ and $|\nabla\phi|^2_{z=u}$ represent forces on the beam due to damping, bending, stretching, and the electric field. The parameter a represents the strength of damping forces on the system, ϵ_0 is the permittivity of free space and d is the undeflected gap spacing. As shown in Fig. 1, a thin insulating layer of thickness h and permittivity σ_1 is attached to the ground plate. The electric potential ϕ, satisfying Eq. (2.1b), is zero on the ground plate and at voltage V on the deflecting membrane so that

$$\phi(-(d+h)) = 0, \qquad \phi(u) = V. \tag{2.1d}$$

The problem is now reduced by recasting Eqs. (2.1) in the dimensionless variables

$$x' = \frac{x}{L} \qquad y' = \frac{y}{L} \qquad z' = \frac{z}{d}, \qquad u' = \frac{u}{d},$$
$$\phi' = \frac{\phi}{V}, \qquad \sigma' = \frac{\sigma}{\sigma_0}$$

and assuming a small aspect ratio configuration, so that $\delta \equiv d/L \ll 1$, where L is a characteristic linear dimension of the domain Ω. Concentrating first on the potential equation (2.1b), the non-dimensional equation for ϕ' satisfies

$$\nabla'\cdot(\sigma'\nabla'\phi') = 0, \qquad -(1+h/d) \le z' \le u'(x', y', t); \tag{2.2a}$$

$$\sigma' = \begin{cases} 1, & -1 \le z' \le u'(x', y', t); \\ \dfrac{\sigma_1}{\sigma_0}, & -(1+h/d) \le z' \le -1 \end{cases} \tag{2.2b}$$

$$\phi'(-(1+h/d)) = 0, \qquad \phi'(u') = 1. \tag{2.2c}$$

In non-dimensional coordinates, we have that

$$\nabla' \equiv \left(\frac{1}{L}\frac{\partial}{\partial x'}, \frac{1}{L}\frac{\partial}{\partial y'}, \frac{1}{d}\frac{\partial}{\partial z'}\right)$$

and therefore problem (2.2) reduces to

$$\frac{\partial^2\phi'_+}{\partial z'^2} + \delta^2\left(\frac{\partial^2\phi'_+}{\partial x'^2} + \frac{\partial^2\phi'_+}{\partial y'^2}\right) = 0, \quad -1 \le z' \le u'; \tag{2.3a}$$

$$\frac{\partial^2\phi'_-}{\partial z'^2} + \delta^2\left(\frac{\partial^2\phi'_-}{\partial x'^2} + \frac{\partial^2\phi'_-}{\partial y'^2}\right) = 0, \quad -1 - \frac{h}{d} \le z' \le -1; \tag{2.3b}$$

$$\phi'_+(u') = 1, \qquad \phi'_+(-1) = \phi'_-(-1),$$
$$\frac{\partial}{\partial z'}\phi'_+(-1) = \frac{\sigma_1}{\sigma_0}\frac{\partial}{\partial z'}\phi'_-(-1), \qquad \phi'_-(-1-d/h) = 0. \tag{2.3c}$$

In the limit where the small aspect ratio $\delta \to 0$, the leading order solution to (2.3) is

$$\phi' = \begin{cases} 1 + \dfrac{z'-u'}{(1+u') + \frac{d\sigma_0}{h\sigma_1}} & -1 \le z' \le u'; \\ \dfrac{z'+1+\frac{d}{h}}{\frac{\sigma_1}{\sigma_0}(1+u') + \frac{d}{h}} & -1-\dfrac{h}{d} \le z' \le -1 \end{cases} \tag{2.4}$$

The explicit solution (2.4) which arises in this small aspect ratio limit affords a significant reduction in the complexity of the governing equations. If the limit $\delta \to 0$ is not exercised, the system for the potential (2.3) and the non-dimensionalized form of (2.1a) constitutes a free boundary problem for the deflection $u(x, y, t)$ of the device. With the exclusion of the insulating layer introduced here in (2.1c), the qualitative properties of dynamic and steady solutions of this free boundary problem have been studied in [31–36]. These studies have established the well-posedness theory for the system of evolution equations (2.1), the existence of a pull in voltage and also the convergence of equilibrium solutions of the free boundary problem to those of the small aspect ratio limit as $\delta \to 0$. Accordingly, there is good reason to believe that the small aspect ratio approximation is justified. In light of the significant simplifications it affords, we proceed by calculating from (2.4) that the forcing on the surface $z' = u'(x', y')$ is given by

$$\frac{\epsilon_0}{2}|\nabla\phi|^2 = V^2\frac{\epsilon_0}{2d^2}\left[\left(\frac{\partial\phi'}{\partial z'}\right)^2 + \mathcal{O}(\delta^2)\right] = V^2\frac{\epsilon_0}{2d^2}\frac{1}{\left(1+u'+\frac{d\sigma_0}{h\sigma_1}\right)^2}. \tag{2.5}$$

After selecting the time scale $t = (L^2 a/T)t'$ in (2.1) and substituting the reduced term arrived at in (2.5), the equation

$$Q^2\frac{\partial^2 u'}{\partial t'^2} + \frac{\partial u'}{\partial t'} + \beta\Delta'^2_\perp u' - \Delta'_\perp u' = -\frac{\lambda}{(1+u'+\varepsilon)^2} \tag{2.6a}$$

is obtained, where the dimensionless groups are

$$\beta = \frac{EI}{L^2 T}, \qquad Q = \frac{\sqrt{T\rho h_0}}{aL}, \qquad \varepsilon = \frac{d\sigma_0}{h\sigma_1},$$
$$\lambda = \frac{\epsilon_0 L^2 V^2}{2d^3 T}. \tag{2.6b}$$

The focus of our attention is further restricted to the case of small quality factor, Q, for which the $Q^2 u_{tt}$ term in (2.6) is considered negligible. This approximation, called the viscous damping limit [23], assumes that inertial effects are negligible compared to those of damping. The consequences of retaining a small $Q > 0$ in (2.6a) have recently been studied in [37,38]. All quantities are now dimensionless and all derivatives are in the x, y directions so the $'$ and $\perp$ notations can be dropped. In summary, the dynamics of a MEMS device in the presence of an insulating layer is thus modeled by the following obstacle problem:

$$u_t = -\beta\Delta^2 u + \Delta u - \frac{d\psi_\varepsilon}{du}, \qquad \psi_\varepsilon(u) = -\frac{\lambda}{1+u+\varepsilon}, \quad x \in \Omega; \tag{2.7a}$$

$$u \ge -1, \quad x \in \Omega; \tag{2.7b}$$

with boundary and initial values

$$u = 0, \quad \partial_n u = 0, \quad \text{on} \quad \partial\Omega; \qquad u = 0, \quad t = 0. \tag{2.7c}$$

The combination of the ε term in the Coulomb nonlinearity of (2.7a) and the obstacle constraint (2.7b), acts to prevent blow up at touchdown.

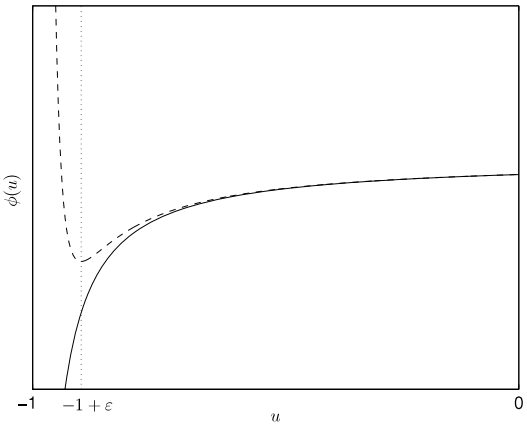

Fig. 2. A schematic diagram of the potential (2.10). The solid line indicates the case $\varepsilon = 0$ while the dashed line represents the case $0 < \varepsilon < 1$. Note that the perturbed potential has the generic features of having a local minimum at $u = -1+\varepsilon$, of being repulsive when $-1 < u < -1+\varepsilon$, and attracting when $u > -1+\varepsilon$.

2.1. Variational nature of the obstacle problem and a regularization

Obstacle problems like (2.7) often arise in mechanics when constraints are present [39]. From a variational point of view, constraints are typically encoded by assigning infinite energy to the set of disallowed configurations. Our model could be written formally as the L^2-gradient flow of the energy functional $E : H^2(\Omega) \to \mathbb{R} \cup \{+\infty\}$ given by

$$E = \int_\Omega \left(\frac{\beta}{2}(\Delta u)^2 + \frac{1}{2}|\nabla u|^2 + \psi(u;\varepsilon) \right) dx\, dy, \tag{2.8}$$

where

$$\psi(u;\varepsilon) = \begin{cases} -\dfrac{\lambda}{1+u+\varepsilon} & u \geq -1, \\ +\infty & u < -1, \end{cases} \tag{2.9}$$

is an extension of ψ_ε in (2.7a) to $u \in \mathbb{R}$.

For practical purposes, it is often useful to work with a regularized version of the obstacle problem which has smooth solutions (e.g. [40,41]). This typically involves, in essence, replacing an energy functional like (2.8) with one which is smooth but otherwise mimics the penalization associated with the obstacle.

For our problem, we will replace the potential (2.9) with one which has the same qualitative structure. Specifically, the new potential ϕ_ε will behave like ψ in the following ways:

1. For fixed values of $u > -1$, $\phi_\varepsilon(u) \sim \psi(u;\varepsilon)$ as $\varepsilon \to 0$.
2. $\lim_{u \to -1^+} \phi_\varepsilon(u) = +\infty$.
3. The value of ψ which occurs at the obstacle value $u = -1$ is the same as the minimum of $\phi_\varepsilon(u)$.

A class of potentials which fulfills these criteria is

$$\phi_\varepsilon(u) = -\frac{\lambda}{(1+u)} + \frac{\lambda(\zeta\varepsilon)^{m-2}}{(m-1)(1+u)^{m-1}}, \tag{2.10}$$
$$\lambda > 0,\ 0 < \varepsilon < 1,$$

for integer exponents $m > 2$, and $\zeta = (m-2)/(m-1)$. We set $\varepsilon' = \zeta\varepsilon$, i.e. the regularizing parameter ε' associated with the potential $\phi_{\varepsilon'}(u)$ is a non-dimensional rescaling of the original physical ε, defined in (2.6b). Hereafter we drop the prime notation. A schematic diagram of the graph of ϕ_ε is shown in Fig. 2.

In the preceding discussion, we have used an elastic model of the deflecting surface based on a plate under tension, which results in a combination of Laplacian and bi-Laplacian terms in (2.7a). Our analysis and observations indicate that when both these terms are present, qualitative solution features such as the scaling properties of solutions as $\varepsilon \to 0$ (cf. Section 4) and the presence of oscillatory boundary layer profiles (cf. Fig. 11), are those associated with the bi-Laplacian only case. To effect a cleaner quantitative analysis, we therefore study equations featuring the bi-Laplacian and Laplacian terms in isolation, rather that in combination. In the bi-Laplacian case we can dispense with the parameter β by a different non-dimensionalization

$$\lambda = \frac{\varepsilon_0 L^4 V^2}{2d^3 EI}, \qquad t = \frac{L^4 a}{EI}\, t', \tag{2.11}$$

whereas for the Laplacian case, the scaling of λ is as in (2.6b).

The culmination of the obstacle regularization and separation of the linear term therefore leads us to study two problems, the second order equation

$$u_t = \Delta u - \frac{\lambda}{(1+u)^2} + \frac{\lambda\varepsilon^{m-2}}{(1+u)^m}, \quad x \in \Omega; \qquad u = 0, \quad x \in \partial\Omega, \tag{2.12a}$$

and the fourth order equation

$$u_t = -\Delta^2 u - \frac{\lambda}{(1+u)^2} + \frac{\lambda\varepsilon^{m-2}}{(1+u)^m}, \quad x \in \Omega; \qquad u = \partial_n u = 0, \quad x \in \partial\Omega. \tag{2.12b}$$

In particular, the singular limit $\varepsilon \to 0$ will receive special attention.

3. Properties of the regularized equations

3.1. Well-posedness

In this section we detail the existence theory for both the Laplacian and bi-Laplacian problems, which we write as

$$u_t = \Delta u - \phi_\varepsilon'(u), \quad x \in \Omega; \qquad u = 0, \quad x \in \partial\Omega; \tag{3.1a}$$

$$u_t = -\Delta^2 u - \phi_\varepsilon'(u) \quad x \in \Omega; \qquad u = \partial_n u = 0, \quad x \in \partial\Omega, \tag{3.1b}$$

together with the initial condition $u(x,0) = u_0(x)$. The spatial domain $\Omega \subset \mathbb{R}^n$ is assumed compact with a sufficiently smooth boundary. We note that the evolution equations are L^2 gradient flows. In particular, if

$$E_L(t) = \int_\Omega \left(\frac{1}{2}|\nabla u|^2 + \phi_\varepsilon(u) \right) dx\, dy, \tag{3.2a}$$

$$E_B(t) = \int_\Omega \left(\frac{1}{2}|\Delta u|^2 + \phi_\varepsilon(u) \right) dx\, dy, \tag{3.2b}$$

it is easily shown that $dE_L/dt \leq 0$ and $dE_B/dt \leq 0$. The following results are proved for a class of potentials ϕ which is fairly general and for which (2.10) is a subset. For both equations we suppose

$$\phi_\varepsilon(u) \in C^1, \quad \phi_\varepsilon(u) \geq \phi_{\min} \text{ for } u \in (-1,\infty), \qquad \phi_\varepsilon(u) < \phi_{\max} \text{ for } u \in (-1+\varepsilon,\infty)\,. \tag{3.3}$$

Additional restrictions for each equation are

$$\phi_\varepsilon'(u) < 0 \quad \text{if } u \in (-1,-1+\varepsilon), \text{ for Eq. (3.1a)}, \tag{3.4a}$$

$$\phi_\varepsilon(u) \sim c(\varepsilon)(1+u)^{-m+1} \quad u \to -1, \text{ for Eq. (3.1b)}. \tag{3.4b}$$

for constant $c(\varepsilon)$.

Theorem 3.1 (*Global Existence—Laplacian Case*)**.** *Suppose that the initial condition satisfies $u_0 \in C^0(\Omega)$ and $u_0 > -1$. Then the solution for (3.1a) exists for all $t > 0$ and $u(x,t) > \min(\inf u_0, -1+\varepsilon)$.*

Proof. Let $u_\pm(t)$ solve the initial value problems

$$\frac{du_\pm}{dt} = -\phi_\varepsilon'(u_\pm), \quad u_-(0) = \inf u_0, \quad u_+(0) = \sup u_0. \tag{3.5}$$

Conditions (3.3) and (3.4a) ensure that $u_\pm$ will exist for all $t > 0$ and $u_\pm > -1$. Furthermore, $u_- > \min(\inf u_0, -1+\varepsilon)$. Standard comparison methods for parabolic equations yield the *a priori* bounds $u_-(t) \le u(x,t) \le u_+(t)$. This guarantees that the solution will exist globally.

Theorem 3.2 (*Global Existence — Bi-Laplacian Case*)**.** *Suppose that the initial condition satisfies $u_0 \in H^2(\Omega) \cap C^0(\Omega)$ and $u_0 > -1$. Then the solution $u(x,t)$ of (3.1b) exists for all $t > 0$, provided $m \ge 3$ in dimension $n = 1$ and $m > 3$ in dimension $n = 2$.*

Proof. Following [42], it suffices to derive *a priori* pointwise bounds on the solution. This guarantees that the equation is uniformly parabolic and existence follows from standard arguments. The gradient flow structure and $dE_B/dt \le 0$ implies that $E_B(T) - E_B(0) \le 0$ for any $T > 0$, and so

$$\int_\Omega \frac{1}{2}(\Delta u(T))^2 dx\,dy \le \int_\Omega \frac{1}{2}(\Delta u_0)^2 dx\,dy + \int_\Omega \phi_\varepsilon(u_0) dx\,dy - \int_\Omega \phi_\varepsilon(u(T)) dx\,dy. \tag{3.6}$$

Since $\phi(\cdot)$ has a lower bound, it follows that $u \in H^2(\Omega)$ *a priori*. The Sobolev embedding theorem then gives $u \in C^1(\Omega)$ in dimension $n = 1$ and $u \in C^{0,\alpha}(\Omega)$ in dimension $n = 2$ where $0 < \alpha < 1$. In particular there are constants K_1 and K_2, depending only on the initial condition, so that

$$\|u\|_{C^1} < K_1, \quad n = 1; \tag{3.7}$$

$$\|u\|_{C^{0,\alpha}} < K_2(\alpha), \quad n = 2. \tag{3.8}$$

Now let $u_{\min} = \min u(T)$ be the minimum attained at a point x_0. Note that inequality (3.6) implies an upper bound for $\int_\Omega \phi_\varepsilon(u(T)) dx\,dy$. In dimension $n = 1$ it follows that there exist generic constants K so that

$$\begin{aligned} C &> \int_\Omega \phi_\varepsilon(u(T)) dx\,dy \\ &\ge K(\varepsilon) \int_\Omega (u_{\min} + 1 + K_1|x - x_0|)^{-m+1} dx\,dy \\ &\ge \mu(u_{\min} + 1), \end{aligned} \tag{3.9}$$

where

$$\mu(u_{\min}+1) = K(\varepsilon) \begin{cases} -\log(u_{\min}+1) & m = 3, \\ (u_{\min}+1)^{-m+3} & m > 3. \end{cases} \tag{3.10}$$

In dimension $n = 2$ one similarly has

$$\begin{aligned} C &> K(\varepsilon) \int_\Omega (u_{\min} + 1 + K_2|x - x_0|^\alpha)^{-m+1} dx\,dy \\ &\ge \mu(u_{\min} + 1), \end{aligned} \tag{3.11}$$

where

$$\mu(u_{\min}+1) = K(\alpha,\varepsilon) \begin{cases} -\log(u_{\min}+1) & m = 1 + 2/\alpha, \\ (u_{\min}+1)^{3-m} & m > 1 + 2/\alpha. \end{cases} \tag{3.12}$$

In both cases, this establishes, for $\varepsilon > 0$, the lower bound $u > -1$ for all $t > 0$.

The two preceding results capture two important features of the perturbed potential system. First, for a wide range of potentials, Eqs. (3.1) mimic the effect of the obstacle constraint $u > -1$, established in (2.7b). This provides confidence that the perturbed potential system qualitatively reflects the behavior of the obstacle problem (2.7). Second, in contrast to the $\varepsilon = 0$ case, the system is now well-posed for all $t > 0$ and $\varepsilon > 0$ and no finite time singularity occurs. It is therefore relevant to investigate the limiting behavior of Eqs. (3.1) in the limit $t \to \infty$. This long term behavior of Eqs. (3.1) is related to the minimizers of the functionals given in (3.2).

3.2. Variational dynamics

The dynamics of Eqs. (2.12) is variational and leads to relaxation of the system towards equilibrium solutions. For values of λ such that touchdown would not occur when $\varepsilon = 0$, the regularization term in (2.12) remains of order ε^{m-2} since $1 + u$ remains finite, and the dynamics in the presence of regularization is therefore a regular perturbation of the dynamics without regularization. For larger values of λ however, the nonlinear term is prevented from diverging by the regularization term and the dynamics evolve towards a solution for which most of the membrane is in near contact with the dielectric layer covering the substrate. This is illustrated in Fig. 3, in the Laplacian case, for a one-dimensional domain, $\Omega = [-1, 1]$. As an initially flat membrane deforms under the effect of the applied electric field, it first touches down at one point in the middle of the domain Ω. A region where $u \simeq -1 + \varepsilon$ then grows from the initial touchdown location towards the boundary of the domain. The spreading of the contact set slows down as its periphery approaches the edge of the domain before eventually being arrested at distances $\pm(1 - x_c)$ from the $x = \pm 1$ boundary points. Qualitatively similar behavior is observed in the bi-Laplacian case. A forthcoming paper [43] will concentrate on quantitative descriptions of the dynamical spreading of the contact set.

This dynamics is markedly different from the $\varepsilon = 0$ case, for which no equilibrium solutions exist above a given threshold $\lambda > \lambda^*$. As we will see below, this is due to the appearance of a new maximal branch of equilibrium solutions when $\varepsilon \ne 0$. Here we define the maximal solution as the one attaining the greatest L^2 norm for any particular λ.

3.3. One-dimensional equilibrium solutions and bifurcation diagrams

One-dimensional equilibrium solutions satisfy the second order elliptic equation

$$u_{xx} = \frac{\lambda}{(1+u)^2} - \frac{\lambda\varepsilon^{m-2}}{(1+u)^m}, \quad x \in (-1,1);\ u(\pm 1) = 0, \tag{3.13a}$$

and its fourth order equivalent

$$-u_{xxxx} = \frac{\lambda}{(1+u)^2} - \frac{\lambda\varepsilon^{m-2}}{(1+u)^m}, \quad x \in (-1,1); \quad u(\pm 1) = u'(\pm 1) = 0. \tag{3.13b}$$

Fig. 4 shows bifurcation diagrams obtained by numerically solving the relevant boundary value problem at fixed values of $\|u\|_2^2$. Starting from $\|u\|_2^2 = 0$, and $\lambda = 0$, a continuation method is employed to trace out each solution branch of the bifurcation diagram by identifying a value of λ and a solution $u(x)$ for each incremental value of the L^2 norm of the solution.

The bifurcation diagrams shown in Fig. 4 exhibit two remarkable deviations from the standard $\varepsilon = 0$ bifurcation diagram, displayed as a dashed curve on both panels. The first is that for λ arbitrarily close to 0 and ε finite, Eqs. (2.12) appear to have a unique equilibrium solution—the minimal solution branch. Secondly, there exists a parameter range where the system exhibits bistability, and thus also possesses a stable maximal branch of

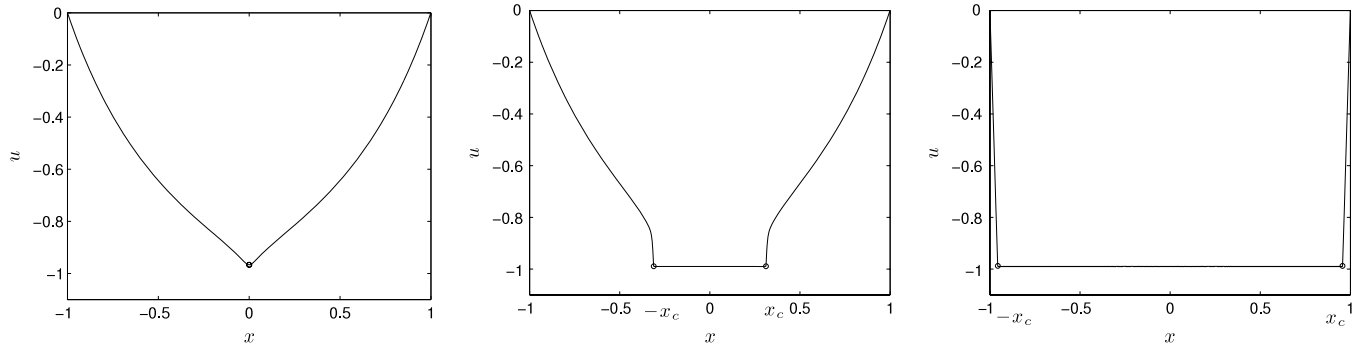

(a) Initial touchdown. (b) Spreading of touchdown region. (c) Boundary pinning.

Fig. 3. One-dimensional solutions of (2.12a) initialized with zero initial data and parameter values $\varepsilon = 0.01$, $\lambda = 5$. The left panel shows the initial touchdown event at $x = 0$. The center panel shows the spread of the touchdown region towards the boundary. Right panel: an equilibrium state is reached after the moving front is pinned by its interaction with the boundary.

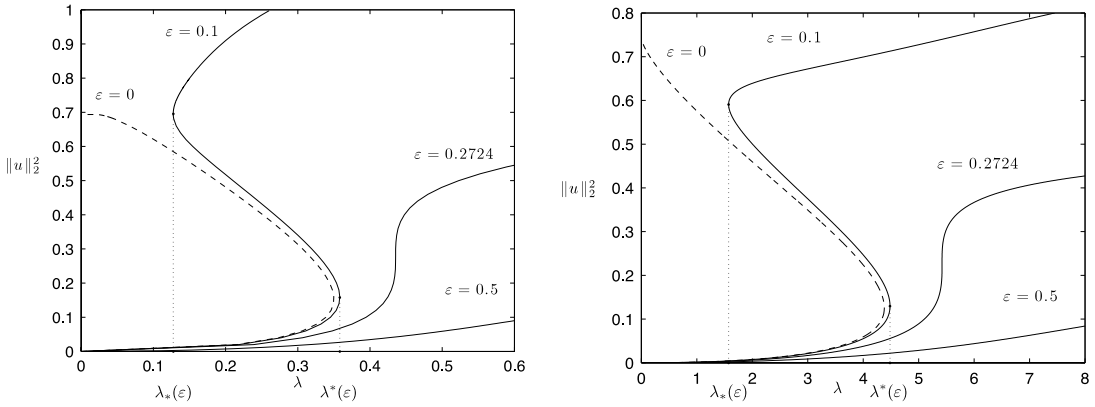

(a) Laplacian bifurcation diagram. (b) Bi-Laplacian bifurcation diagram.

Fig. 4. Numerically obtained bifurcation diagrams showing equilibrium solutions of (2.12) for $m = 4$. Left panel: Laplacian case; right panel: bi-Laplacian case. In each of the above, solution curves are plotted for $\varepsilon < \varepsilon_c$, $\varepsilon \approx \varepsilon_c$ and $\varepsilon > \varepsilon_c$ to highlight the threshold of bistability. When $\varepsilon = 0$, only two branches of solutions exist (dashed curves).

equilibrium solutions. More precisely, there is a critical value ε_c such that for $\varepsilon < \varepsilon_c$, Eqs. (2.12) are bistable over a parameter range $0 < \lambda_*(\varepsilon) < \lambda < \lambda^*(\varepsilon)$ while for $\varepsilon \geq \varepsilon_c$, a unique solution is present for each λ, including for large values of λ. As $\varepsilon \to 0$, the bistable region extends towards smaller values of λ, that is $\lambda_*(\varepsilon) \to 0$, as is further discussed below and in Section 4.3.

3.4. Existence of a new branch of equilibrium solutions

To understand the existence of the saddle–node bifurcation at $\lambda = \lambda_*(\varepsilon)$ when $\varepsilon \neq 0$, we consider the dynamical system describing equilibrium solutions of Eq. (2.12a), with and without regularization. Equilibrium solutions of (2.12a) satisfy (3.13a), which in terms of the rescaled independent variable $y = \sqrt{\lambda}x$ reads

$$u_{yy} = \frac{1}{(1+u)^2} - \frac{\varepsilon^{m-2}}{(1+u)^m}, \quad y \in [-\sqrt{\lambda}, \sqrt{\lambda}], \; u(\pm\sqrt{\lambda}) = 0.$$

The above ordinary differential equation is equivalent to the first-order system

$$\begin{cases} u_y = w \\ w_y = \dfrac{1}{(1+u)^2} - \dfrac{\varepsilon^{m-2}}{(1+u)^m}. \end{cases} \tag{3.14}$$

When $\varepsilon = 0$, this system has a line of singularities at $u = -1$. When $\varepsilon \neq 0$, this line still persists, but trajectories originating near $u = 0$ cannot get close to $u = -1$, due to the presence of a saddle point at $u = -1 + \varepsilon$, $w = 0$ (see Fig. 5). We are interested in trajectories that connect the vertical line $u = 0$ to itself. Amongst these, those of half-length $\sqrt{\lambda}$, if any, correspond to equilibrium solutions of (3.13a). Note that system (3.14) is left invariant by the transformation $y \to -y$, $w \to -w$, and that the equilibrium solutions we are looking for are therefore symmetric with respect to the $w = 0$ axis. One can parameterize each trajectory that connects $u = 0$ to itself by the w-coordinate of the point where the trajectory meets the line $u = 0$ in the upper half-plane, or equivalently by the u-coordinate of the point where the trajectory crosses the horizontal axis. We will denote the former by w_0 and the latter by $u_0 \equiv -1 + \alpha$, with $0 < \alpha \leq 1$. Since distinct trajectories do not cross, w_0 is a decreasing function of α with $\alpha \in (0, 1]$ for $\varepsilon = 0$ and $\alpha \in (\varepsilon, 1]$ for $\varepsilon \neq 0$.

A trajectory that connects the point $(u = -1 + \alpha, w = 0)$ to the point $(u = 0, w = w_0)$ has an equation of the form

$$\frac{1}{2}w^2 = -\frac{1}{1+u} + \frac{\varepsilon^{m-2}}{(m-1)(1+u)^{m-1}} + C,$$
$$C = \frac{1}{\alpha} - \frac{\varepsilon^{m-2}}{(m-1)\alpha^{m-1}},$$

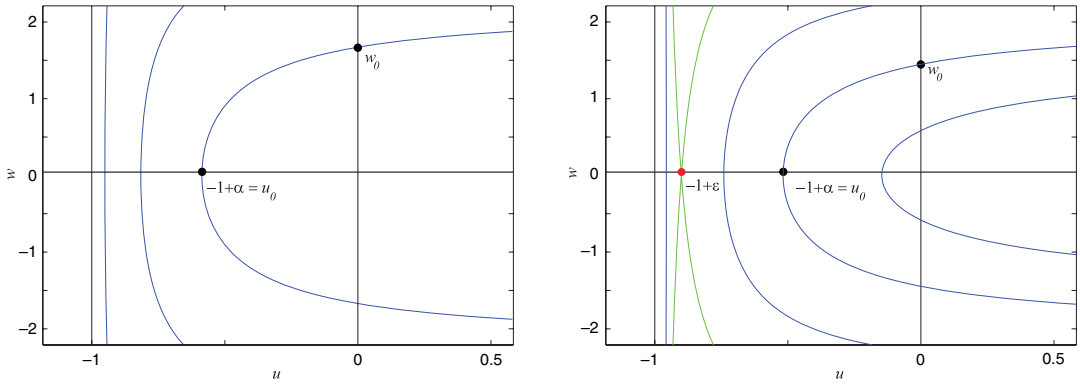

Fig. 5. Phase portraits for the time-independent system in the Laplacian case. Left: no regularization, $\varepsilon = 0$. Right: in the presence of regularization, with $m = 4$, and $\varepsilon = 0.1$. (Trajectories obtained with PPLANE).

and its length $l_\varepsilon(\alpha)$ is given by

$$\begin{aligned} l_\varepsilon(\alpha) &= \int_0^{l(\alpha)} dy = \int_{-1+\alpha}^{0} \frac{du}{w} \\ &= \int_{-1+\alpha}^{0} \left[\left(\frac{1}{\alpha} - \frac{1}{1+u} \right) + \frac{\varepsilon^{m-2}}{m-1} \right. \\ &\quad \left. \times \left(\frac{1}{(1+u)^{m-1}} - \frac{1}{\alpha^{m-1}} \right) \right]^{-1/2} du. \end{aligned} \tag{3.15}$$

When $\varepsilon = 0$, the above integral can easily be evaluated as

$$\begin{aligned} l_0(\alpha) &= \left[\sqrt{\frac{\alpha}{2}} \left(\sqrt{(1+u)(1+u-\alpha)} \right. \right. \\ &\quad \left. \left. + \alpha \log \left(\sqrt{1+u} + \sqrt{1+u-\alpha} \right) \right) \right]_{-1+\alpha}^{0} \\ &= \sqrt{\frac{\alpha}{2}} \left(\sqrt{1-\alpha} + \alpha \log \left(1 + \sqrt{1-\alpha} \right) - \alpha \log \left(\sqrt{\alpha} \right) \right). \end{aligned}$$

As shown in Fig. 6, for $\alpha \in (0, 1]$, the graph of the above function is concave down with $l_0(1) = 0$ and $\lim_{\alpha \to 0^+} l_0(\alpha) = 0$. It has a maximum at $\alpha^*(0) \simeq 0.612$. As a consequence, for values of λ such that $\sqrt{\lambda} < l_0(\alpha^*(0))$, there are two branches of solutions that satisfy the boundary conditions. These two branches meet at a saddle–node bifurcation when $\lambda = \lambda^*(0) = l_0(\alpha^*(0))^2 \simeq 0.35$. This value of λ agrees very well with the numerically obtained value of the turning point for the bifurcation diagram of Fig. 4 with $\varepsilon = 0$ (dashed curve in left panel).

For $\varepsilon \neq 0$, the change of variable $v = \frac{u+1-\alpha}{\alpha}$ leads to

$$\begin{aligned} l_\varepsilon(\alpha) &= \frac{\alpha^{3/2}}{\sqrt{2}} \int_0^{-1+1/\alpha} \left[\frac{v}{v+1} \right. \\ &\quad \left. + \frac{\varepsilon^{m-2}}{(m-1)\alpha^{m-2}} \frac{1-(1+v)^{m-1}}{(1+v)^{m-1}} \right]^{-1/2} dv \\ &= \frac{\alpha^{3/2}}{\sqrt{2}} \int_0^{-1+1/\alpha} \left(\frac{v}{v+1} \right)^{-1/2} \\ &\quad \times \left[1 + \frac{\varepsilon^{m-2}}{(m-1)\alpha^{m-2}} \frac{1-(1+v)^{m-1}}{v(1+v)^{m-2}} \right]^{-1/2} dv. \end{aligned}$$

The above integral may be expanded in powers of ε near $\alpha = \mathcal{O}(1)$. Since

$$1 \leq \frac{(1+v)^{m-1}-1}{v(1+v)^{m-2}} \leq m-1 \quad \text{for } v \geq 0,$$

the integral appearing in the k-th term of the expansion is finite, and we therefore obtain a regular asymptotic expansion of $l_\varepsilon(\alpha)$ in powers of ε. For α near α^*, this expansion may be used to describe how the location of the saddle–node bifurcation that occurs at $\lambda = \lambda^*(0)$ when $\varepsilon = 0$ is modified for small values of ε. We indeed obtain

$$\begin{aligned} \lambda^*(\varepsilon) &= l_\varepsilon(\alpha^*(\varepsilon))^2 \\ &= \lambda^*(0) + \varepsilon^{m-2} \frac{[\alpha^*(0)]^{-m+7/2}}{m-1} \sqrt{\frac{\lambda^*(0)}{2}} \\ &\quad \times \int_0^{-1+1/\alpha} \left(\frac{v}{v+1} \right)^{-1/2} \frac{(1+v)^{m-1}-1}{v(1+v)^{m-2}} dv \\ &\quad + \mathcal{O}\left(\varepsilon^{2(m-2)} \right), \end{aligned}$$

where $\alpha^*(\varepsilon)$ is the value of α at which $l_\varepsilon(\alpha)$ reaches its local maximum. For $m = 4$, the above reads $\lambda^*(\varepsilon) \simeq 0.350004 + 0.794451\varepsilon^2 + \mathcal{O}\left(\varepsilon^4\right)$, which is in agreement with the expansion of $\lambda^*(\varepsilon)$ briefly mentioned in Section 4, and derived in [44].

As $\alpha \to \varepsilon^+$, $l_\varepsilon(\alpha)$ is expected to diverge for all values of $\varepsilon \neq 0$, since the trajectory approaches the fixed point at $u = -1 + \varepsilon$, $w = 0$. To analyze this divergence, we set $\alpha = \kappa\varepsilon$, with $\kappa = 1 + \eta$ and η small, and obtain

$$\begin{aligned} l_\varepsilon(\alpha) &= \frac{\alpha^{3/2}}{\sqrt{2}} \int_0^{-1+1/\alpha} \left(\frac{v}{v+1} \right)^{-1/2} \\ &\quad \times \left[g(\eta) + \frac{v\, p(v)}{(1+v)^{m-2}} \right]^{-1/2} dv, \end{aligned}$$

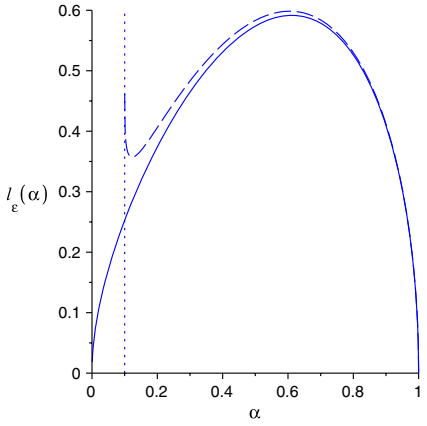

Fig. 6. Graph of the function $l_\varepsilon(\alpha)$ in the harmonic case in the absence of regularization ($\varepsilon = 0$, solid curve) and in the presence of regularization (for $\varepsilon = 0.1$ with $m = 4$, dashed curve). The vertical line at $\alpha = \varepsilon = 0.1$ indicates where $l_\varepsilon(\alpha)$ diverges when $\varepsilon \neq 0$.

where

$$g(\eta) = \frac{1}{(1+\eta)^{m-2}} \sum_{k=1}^{m-2} \binom{m-2}{k} \eta^k$$

$$v\,p(v) = \frac{1}{(1+\eta)^{m-2}} \sum_{k=1}^{m-2} \binom{m-2}{k} \frac{k}{k+1} v^k.$$

The function $H(v) = \frac{v\,p(v)}{(1+v)^{m-2}}$ is such that $H(0) = 0$ and

$$\lim_{v\to\infty} H(v) = \frac{1}{(1+\eta)^{m-2}} \frac{m-2}{m-1}.$$

Moreover, H is strictly increasing for $0 \le v \le L$, with $L = -1 + 1/\alpha$; a simple calculation indeed shows that its derivative is given by

$$\frac{dH}{dv} = \frac{1}{(1+\eta)^{m-2}} \frac{1}{(1+v)^{m-1}} \left[\frac{m-2}{2} + \sum_{k=1}^{m-3} \binom{m-2}{k+1} \frac{v^k}{k+2} \right] \ge \frac{m-2}{2(1+\eta)^{m-2}}.$$

As a consequence, on the interval $[0, L]$, H is bounded above by the line tangent to its graph at the origin, and bounded below by the straight line that goes through the origin and the point of coordinates $(L, H(L))$. In other words,

$$\frac{p(L)v}{(1+L)^{m-2}} \le H(v) \le \frac{(m-2)v}{2(1+\eta)^{m-2}}, \quad 0 \le v \le L.$$

This, together with $1 \le v+1 \le L+1$ for $v \in [0, L]$, allows us to bound the term $\left[g(\eta) + \frac{v\,p(v)}{(1+v)^{m-2}} \right]^{-1/2}$ that appears in the expression for $l_\varepsilon(\alpha)$, and therefore bound $l_\varepsilon(\alpha)$. Noting that

$$\int \frac{dv}{\sqrt{v(v+s(\eta))}} = 2\log\left(\sqrt{v} + \sqrt{v+s(\eta)} \right),$$

we obtain $l_<(\eta) \le l_\varepsilon(\alpha) \le l_>(\eta)$, where $\eta = \frac{\alpha}{\varepsilon} - 1$ and

$$\begin{aligned} l_<(\eta) &= \frac{\varepsilon^{3/2}}{\sqrt{m-2}} \left(1 + \frac{m+1}{2}\eta + \mathcal{O}(\eta^2) \right) \\ &\quad \times \log\left(\frac{2(1-\varepsilon)}{\varepsilon\eta} + \frac{m-3}{2}\eta + \mathcal{O}(\eta^2) \right) \\ l_>(\eta) &= -\frac{\varepsilon^{1/2}}{\sqrt{2}} \sqrt{\frac{m-1}{m-2}} \log(g(\eta)) \\ &\quad + \mathcal{O}\left((\eta+\varepsilon)(\log(\eta) + \log(\varepsilon)) \right). \end{aligned}$$

For ε fixed but small and $\eta \to 0$, we thus have

$$-\frac{\varepsilon^{3/2}}{\sqrt{m-2}} \log(\eta) + \mathcal{O}\left(\eta \log(\eta)\right) \le l_\varepsilon(\alpha) \le -\frac{\varepsilon^{1/2}}{\sqrt{2}} \sqrt{\frac{m-1}{m-2}} \log(\eta) + \mathcal{O}\left(\eta \log(\eta)\right). \tag{3.16}$$

This indicates that the graph of $l_\varepsilon(\alpha)$ initially follows that of $l_0(\alpha)$ as α decreases towards ε, and then diverges likes $-\log(\eta) = -\log(-1 + \alpha/\varepsilon)$, as shown in Fig. 6. The dashed curve is a numerical evaluation of $l_\varepsilon(\alpha)$ for $\varepsilon = 0.1$ and $m = 4$. This divergence as $\alpha \to \varepsilon^+$ implies the existence of a third branch of solutions for $\lambda \ge \lambda_*(\varepsilon)$, where $\sqrt{\lambda_*(\varepsilon)}$ is the local minimum of $l_\varepsilon(\alpha)$. The bounds in Eq. (3.16) show that $\sqrt{\lambda_*(\varepsilon)} \to 0$ as $\varepsilon \to 0^+$. As ε increases, the minimum of the graph of $l_\varepsilon(\alpha)$ merges with its maximum, and only one branch of solutions exists beyond that point. This is illustrated in the numerically obtained bifurcation diagrams shown in Fig. 4 with $\varepsilon \neq 0$ (solid curves in the left panel). The right panel of Fig. 4 shows that a similar behavior is observed in the bi-Laplacian case.

3.5. Nature of the new branch of solutions

The newly present maximal branch of stable equilibria can be interpreted as a post touchdown equilibrium state. These additional solutions have three characteristic features, as illustrated in Fig. 7 for values of $\lambda > \lambda_*$. First, in a large central portion of the domain, the solution is flat and takes on values near $-1+\varepsilon$. Second, a sharp transition layer links the flat region to a profile satisfying the boundary conditions. For the Laplacian problem (3.13a), this sharp interface is monotone while in the bi-Laplacian case, the profile is non-monotone. Therefore, in the Laplacian case the region where $u \simeq -1+\varepsilon$ is spread over a finite interval while in the bi-Laplacian case, u attains its minimum only at two discrete points. The third characteristic feature of this branch of equilibrium solutions is the nature of the profile connecting the boundary to the transition layer and in particular the size of the boundary layer. In what follows, we use matched asymptotic expansions to characterize these properties in the limit as $\varepsilon \to 0$.

4. Scaling properties of equilibrium solutions.

In this section, we construct 1D post-touchdown equilibrium configurations of (3.13) in the limit as $\varepsilon \to 0$. As seen in Fig. 7, these solutions have interfaces located at $\pm x_c$, around which a narrow transition layer is centered. This transition layer separates an interior region of finite extent $(-x_c, x_c)$, from a sharp boundary profile. As explained above, the deflection profile u satisfies $u(x) = -1 + \mathcal{O}(\varepsilon)$ in the entire interior region, is monotonic on $[0, 1]$ in the Laplacian case, and has a local minimum at the discrete points $\pm x_c$ in the bi-Laplacian case. In both cases, it is necessary to calculate the extent of the interior region $(-x_c, x_c)$. From numerical simulations, it appears that x_c approaches the boundary as $\varepsilon \to 0$. In the calculations below, we impose this condition, determine the scaling laws that ensue, and find the equilibrium solutions in terms of matched asymptotic expansions.

4.1. Laplacian case

We consider Eqs. (3.13a) in the limit $\varepsilon \to 0$ and look for solutions to

$$u_{xx} = \frac{\lambda}{(1+u)^2} - \frac{\varepsilon^{m-2}\lambda}{(1+u)^m}, \quad x \in [-1, 1]; \tag{4.1a}$$

$$u(\pm 1) = 0, \tag{4.1b}$$

that satisfy the following properties: (i) $u(x) = -1 + \varepsilon + \sigma(\varepsilon)$ for $x \in [-x_c, x_c]$, (ii) $u(x)$ goes from its interior value of $-1+\varepsilon+\sigma(\varepsilon)$ to the value 1 in the boundary layers $[-1, -x_c]$ and $[x_c, 1]$, and (iii) there are two transition regions, centered at $\pm x_c$. From a dynamical system point of view, the particular trajectory we are interested in crosses the horizontal axis $w = u_x = 0$ of the associated phase plane near but to the right of the fixed point $(-1+\varepsilon, 0)$. As the trajectory gets closer to the fixed point $(-1+\varepsilon, 0)$, the corresponding solution $u(x)$ "spends more time" near $u = -1+\varepsilon$ and therefore $x_c \to 1$. To make the scaling explicit, we write $x_c = 1 - \varepsilon^p \bar{x}_c$ for some $\bar{x}_c$ and p to be determined. From symmetry considerations, since $\Omega = [-1, 1]$, we need only study the equations on the interval $[0, 1]$.

To analyze the solution in the boundary layer interval $[1 - \varepsilon^p \bar{x}_c, 1]$, it is convenient to use the variables

$$u(x) = w(\eta), \qquad \eta = \frac{x - x_c}{1 - x_c} = \frac{x - (1 - \varepsilon^p \bar{x}_c)}{\varepsilon^p \bar{x}_c}, \tag{4.2}$$

which transform (4.1) and the boundary condition $u(1 - \varepsilon^p \bar{x}_c) = -1 + \mathcal{O}(\varepsilon)$ into

$$w_{\eta\eta} = \varepsilon^{2p} \lambda_c \left[\frac{1}{(1+w)^2} - \frac{\varepsilon^{m-2}}{(1+w)^m} \right], \quad \eta \in [0, 1]; \tag{4.3a}$$

$$w(0) = -1 + \mathcal{O}(\varepsilon), \quad w(1) = 0,$$

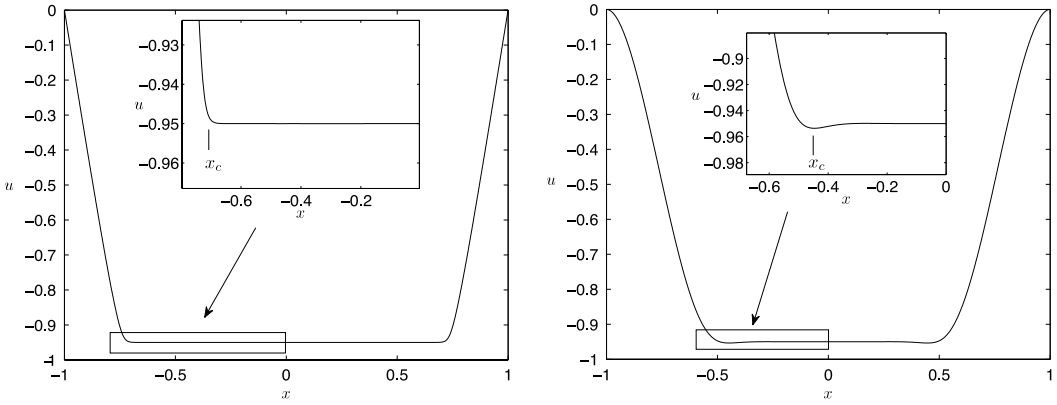

(a) Second order, $\varepsilon = 0.05$, $\lambda = 0.63$. (b) Fourth order, $\varepsilon = 0.05$, $\lambda = 24.82$.

Fig. 7. Typical solutions of (3.13) on the stable upper branch for $m = 4$. Panels (a) and (b) represent solutions of (3.13a) and (3.13b) respectively. In each of the two panels, the inset panels show an enlargement of the sharp interface and touchdown region.

where we have defined

$$\lambda_c = \lambda \bar{x}_c^2. \tag{4.3b}$$

In light of Eq. (4.4b) below, the introduction of λ_c should be viewed as equivalent to expanding x_c in powers of ε and $\varepsilon \log \varepsilon$. We now develop the asymptotic expansion

$$w = w_0 + \varepsilon^{2p} \log \varepsilon \, w_{1/2} + \varepsilon^{2p} w_1 + \sigma(\varepsilon^{2p}) \tag{4.4a}$$

$$\lambda_c = \lambda_{0c} + \varepsilon^{2p} \log \varepsilon \, \lambda_{1c} + \varepsilon^{2p} \lambda_{2c} + \sigma(\varepsilon^{2p}) \tag{4.4b}$$

for solutions to (4.3a). The $\mathcal{O}(\varepsilon \log \varepsilon)$ terms are known as logarithmic switchback terms and have previously appeared in the asymptotic construction of singular solutions to non-regularized MEMS problems [45]. Their necessity in obtaining a consistent expansion is due to a logarithmic singularity in w_1 and will become apparent in the process of matching to a local solution valid in the vicinity of $\eta = 0$. At leading order, the solution is given by $w_0(\eta) = -1 + \eta$ while the switchback term satisfies $w_{1/2} = a_{1/2}(\eta - 1)$ where $a_{1/2}$ is a constant to be determined in the matching process. The problem for w_1 is

$$w_{1\eta\eta} = \frac{\lambda_{0c}}{(1 + w_0)^2}, \quad 0 < \eta \leq 1; \qquad w_1(1) = 0, \tag{4.5a}$$

and its solution reads

$$w_1 = -\lambda_{0c} \log \eta + a_1(\eta - 1). \tag{4.5b}$$

In the transition layer near $\eta = 0$, i.e. for $x \simeq x_c$, we introduce the local variables

$$w(\eta) = -1 + \varepsilon^{v} v(\xi), \qquad \xi = \frac{x - x_c}{\varepsilon^{q}}, \tag{4.6}$$

and set the values $v = 1$ and $q = 3/2$. This transforms Eq. (4.3a) to

$$v_{\xi\xi} = \varepsilon^{2p-1} \lambda \left[\frac{1}{v^2} - \frac{1}{v^m} \right], \quad -\infty < \xi < \infty. \tag{4.7}$$

To balance the left and right hand sides of (4.7) as $\varepsilon \to 0$, the value $p = 1/2$ is required. In order to match with the far-field solutions, we need to impose

$$\lim_{\xi \to -\infty} v(\xi) = 1 + \sigma(1);$$

$$-1 + \varepsilon v\left(\frac{\eta \bar{x}_c}{\varepsilon} \right) \sim w(\eta) \quad \text{as } \xi = \frac{\eta \bar{x}_c}{\varepsilon} \to \infty.$$

Since the associated dynamical system has only one fixed point at (1,0) in the (v, v_ξ) phase plane, there is no trajectory that exactly meets these conditions. However, the unstable manifold of the above fixed point satisfies the zeroth order equation and boundary conditions. We then look for approximate solutions that solve the differential equation to a given order in ε and also have the correct behavior as $\xi \to -\infty$, to the same order in ε. In particular, if the $\sigma(\varepsilon)$ term that appears in the boundary condition is small beyond all orders in ε, we will have $v(\xi) = v_0(\xi) + \sigma(\varepsilon^k)$, for all integers $k \geq 1$. The leading order problem for $v_0(\xi)$ reads

$$v_{0\xi\xi} = \lambda \left[\frac{1}{v_0^2} - \frac{1}{v_0^m} \right], \quad -\infty < \xi < \infty, \tag{4.8a}$$

$$v_0(\xi) \to 1, \quad v_{0\xi}(\xi) \to 0, \quad \text{as } \xi \to -\infty. \tag{4.8b}$$

As mentioned above, its solution corresponds to the positive branch of the unstable manifold of the fixed point $(v_0 = 1, v_{0\xi} = 0)$ in the $(v_0, v_{0\xi})$ phase plane of the associated dynamical system. The above equation may be integrated once to give

$$\frac{1}{2} v_{0\xi}^2 = \lambda \left[-\frac{1}{v_0} + \frac{1}{(m-1) v_0^{m-1}} \right] + C_0, \qquad C_0 = \lambda \frac{m-2}{m-1},$$

where the value of C_0 was obtained from the condition as $\xi \to -\infty$. From this equation, we can infer the behavior of the unstable manifold as $\xi \to \infty$: setting $v_0(\xi) = \alpha \xi + \beta \log \xi + \mathcal{O}(1)$ and equating the constant terms and the terms in $1/\xi$, we find

$$v_0(\xi) = \sqrt{\frac{2\lambda(m-2)}{m-1}} \xi - \frac{m-1}{2(m-2)} \log \xi + \gamma + \mathcal{O}\left(\frac{\log \xi}{\xi} \right) \quad \text{as } \xi \to \infty.$$

To match with the boundary layer expansion, we re-write $-1 + \varepsilon v_0(\xi) + \mathcal{O}(\varepsilon)$ in terms of $\eta = \varepsilon \xi / \bar{x}_c$ and obtain, after making use of

$$\bar{x}_c = \sqrt{\frac{\lambda_c}{\lambda}} = \sqrt{\frac{\lambda_{0c}}{\lambda}} \left[1 + \frac{\lambda_{1c}}{\lambda_{0c}} \varepsilon \log \varepsilon + \frac{\lambda_{2c}}{\lambda_{0c}} \varepsilon + \sigma(\varepsilon) \right]^{1/2},$$

the following expansion, as $\xi \to \infty$:

$$\begin{aligned} -1 + \varepsilon v_0(\xi) \simeq\ & -1 + \eta \sqrt{\frac{2\lambda_{0c}(m-2)}{m-1}} \\ & + \eta \sqrt{\frac{2\lambda_{0c}(m-2)}{m-1}} \frac{\lambda_{1c}}{2\lambda_{0c}} \varepsilon \log \varepsilon + \frac{m-1}{2(m-2)} \varepsilon \log \varepsilon \\ & - \frac{m-1}{2(m-2)} \varepsilon \log \eta + \varepsilon \left(\sqrt{\frac{2\lambda_{0c}(m-2)}{m-1}} \frac{\lambda_{2c}}{2\lambda_{0c}} \eta \right. \\ & \left. + \gamma - \frac{m-1}{4(m-2)} \log\left(\frac{\lambda_{0c}}{\lambda} \right) \right) \\ & + \sigma(\varepsilon). \end{aligned}$$

To match with

$$w(\eta) = -1 + \eta + \varepsilon \log \varepsilon\, a_{1/2}(\eta - 1) - \lambda_{0c}\varepsilon \log \eta + \varepsilon a_1(\eta - 1) + \sigma(\varepsilon),$$

we need to impose

$$\lambda_{0c} = \frac{m-1}{2(m-2)}. \tag{4.9}$$

We then have

$$-1 + \varepsilon v_0(\xi) \simeq -1 + \eta + \varepsilon \log \varepsilon \left(\eta \frac{\lambda_{1c}}{2\lambda_{0c}} + \lambda_{0c}\right) - \lambda_{0c}\varepsilon \log \eta + \varepsilon\left(\frac{\lambda_{2c}}{2\lambda_{0c}}\eta + \gamma - \frac{\lambda_{0c}}{2}\log\left(\frac{\lambda_{0c}}{\lambda}\right)\right) + \sigma(\varepsilon),$$

which also requires that

$$a_{1/2} = -\lambda_{0c}, \qquad \lambda_{1c} = -2\lambda_{0c}^2, \qquad \lambda_{2c} = 2a_1\lambda_{0c},$$

and $\quad a_1 = \dfrac{\lambda_{0c}}{2}\log\left(\dfrac{\lambda_{0c}}{\lambda}\right) - \gamma.$

From (4.3b), the two term expansion of $\bar{x}_c$ is then

$$\bar{x}_c = \left[\frac{\lambda_{0c}}{\lambda} - 2\varepsilon \log \varepsilon \frac{\lambda_{0c}^2}{\lambda} + \frac{2a_1\lambda_{0c}}{\lambda}\varepsilon + \sigma(\varepsilon)\right]^{1/2} = \sqrt{\frac{\lambda_{0c}}{\lambda}}\left[1 - \lambda_{0c}\varepsilon \log \varepsilon + a_1\varepsilon + \sigma(\varepsilon)\right]. \tag{4.10}$$

To summarize, we expect the equilibrium solution u of (3.13a) to satisfy the following properties in the limit $\varepsilon \to 0$:

- $u(x) = -1 + \varepsilon + \sigma(\varepsilon^k)$, $k > 2$ in the interior region $x \in [0, x_c]$, with $x_c = 1 - \varepsilon^{1/2}\bar{x}_c$ and $\bar{x}_c$ given by (4.10);
- $u(x) = -1 + \varepsilon\, v_0(\xi) + \sigma(\varepsilon)$ in the transition layer near x_c, with $\xi = \frac{x - x_c}{\varepsilon^{3/2}}$.
- $u(x) = -1 + \eta - \varepsilon \log \varepsilon \lambda_{0c}(\eta - 1) - \lambda_{0c}\varepsilon \log \eta + \varepsilon a_1(\eta - 1) + \sigma(\varepsilon)$ in the boundary layer $x \in (x_c, 1]$, with $\eta = \frac{x - x_c}{\varepsilon^{1/2}\bar{x}_c}$ and $\bar{x}_c$ given by (4.10).

Fig. 8 shows a comparison between the above composite asymptotic expansion and a numerical solution of the full problem, indicating very good agreement. In order to plot the solution obtained with matched asymptotic expansions, we have assumed that the contact point x_c coincides with the maximum of the second derivative of $u(x)$, i.e.,

$$x_c = \arg\max_{x \in [0,1]} u''(x) = (x \in [0, 1] \mid u''(x) = \max_{y \in [0,1]} u''(y)),$$

and calculated numerically the value of γ in (4.10) accordingly.

For comparison to the bifurcation diagrams, the squared L^2 norm of the equilibrium solution to (3.13a) is computed to be, in the limit $\varepsilon \to 0$,

$$\int_{-1}^{1} u(x)^2\, dx = 2\left[\int_0^{1-\varepsilon^{1/2}\bar{x}_c} u(x)^2\, dx + \int_{1-\varepsilon^{1/2}\bar{x}_c}^{1} u(x)^2\, dx\right] = 2\left[1 - 2\varepsilon + \sigma(\varepsilon) - \frac{2}{3}\varepsilon^{1/2}\sqrt{\frac{\lambda_{0c}}{\lambda}} + \sigma(\varepsilon^{3/2}\log\varepsilon)\right].$$

If we replace λ_{0c} by its expression given in (4.9), the above equation reads

$$\|u\|_2^2 = 2\left[1 - \frac{2}{3}\sqrt{\frac{m-1}{2\lambda(m-2)}}\,\varepsilon^{1/2} - 2\varepsilon + \mathcal{O}(\varepsilon^{3/2}\log\varepsilon)\right]. \tag{4.11}$$

The dashed curve in the left panel of Fig. 9 shows the above quantity as a function of λ for $m = 4$ and $\varepsilon = 0.01$, and matches the upper branch of the bifurcation diagram very well. The right panel of Fig. 9 is a numerical confirmation of the $p = 1/2$ scaling.

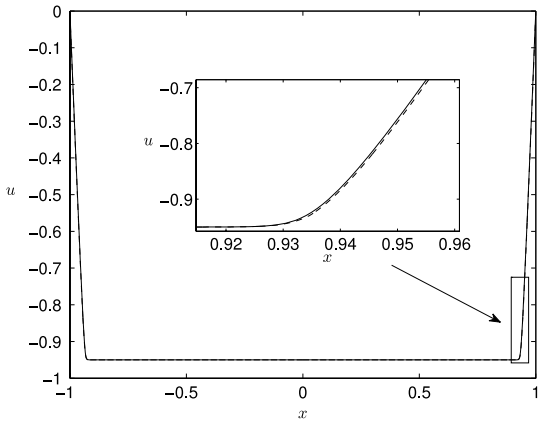

Fig. 8. Composite asymptotic expansion of equilibrium solutions to (4.1) for values $m = 4$, $\lambda = 10$, $\varepsilon = 0.05$. The solid line is the numerical solution and the dashed line is the composite asymptotic expansion.

4.2. Bi-Laplacian case

We now turn to 1D equilibrium profiles of (3.13b) in the limit $x_c \to 1$ as $\varepsilon \to 0$. As in the Laplacian case, we write $x_c = 1 - \varepsilon^p\bar{x}_c$ where p and $\bar{x}_c$ are parameters to be determined. For this particular case, a balancing argument will provide the value $p = 1/4$. We consider the outer solution in the interval $[1 - \varepsilon^p\bar{x}_c, 1]$ and employ the rescaling

$$u(x) = w(\eta), \qquad \eta = \frac{x - (1 - \varepsilon^p\bar{x}_c)}{\varepsilon^p\bar{x}_c}, \tag{4.12}$$

which results in

$$-w_{\eta\eta\eta\eta} = \varepsilon^{4p}\lambda_c\left[\frac{1}{(1+w)^2} - \frac{\varepsilon^{m-2}}{(1+w)^m}\right], \quad \eta \in [0, 1]; \tag{4.13a}$$

$$w(0) = -1, \quad w'(0) = 0, \quad w(1) = w'(1) = 0, \tag{4.13b}$$

where in addition, the parameter λ_c is defined by

$$\lambda_c = \lambda\bar{x}_c^4. \tag{4.13c}$$

A logarithmic singularity also arises in the fourth order case, and as before, switchback terms are required in the expansion of (4.13). In addition there is a term at $\mathcal{O}(\varepsilon^{1/2})$ which arises from the translation invariance of the inner problem. In the end, the expansions

$$w = w_0 + \varepsilon^{1/2}w_{1/4} + \varepsilon^{4p}\log\varepsilon\, w_{1/2} + \varepsilon^{4p}\, w_1 + \sigma(\varepsilon^{4p}); \tag{4.14a}$$

$$\lambda_c = \lambda_{0c} + \varepsilon^{1/2}\lambda_{1c} + \varepsilon^{4p}\log\varepsilon\,\lambda_{2c} + \mathcal{O}(\varepsilon^{4p}) \tag{4.14b}$$

are applied to (4.13). At leading order $w_{0\eta\eta\eta\eta} = 0$ and, with boundary conditions applied, reduces to $w_0 = -1 + 3\eta^2 - 2\eta^3$. The switchback term $w_{1/2}$ solves the problem

$$w_{1/2\eta\eta\eta\eta} = 0, \quad \eta \in (0, 1); \qquad w_{1/2}(1) = w_{1/2\eta}(1) = 0 \tag{4.15a}$$

and is given by

$$w_{1/2}(\eta) = \alpha_1 + \alpha_2\eta - (3\alpha_1 + 2\alpha_2)\eta^2 + (2\alpha_1 + \alpha_2)\eta^3 \tag{4.15b}$$

where α_1 and α_2 are constants to be determined by matching. The term $\varepsilon^{1/2}w_{1/4}$, not present in the Laplacian analysis of Section 4.1, satisfies

$$w_{1/4\eta\eta\eta\eta} = 0, \quad \eta \in (0, 1);$$

$$w_{1/4}(0) = w_{1/4}(1) = w_{1/4\eta}(1) = 0 \tag{4.16a}$$

$$w_{1/4}(\eta) = \xi_0(\eta - 2\eta^2 + \eta^3), \tag{4.16b}$$

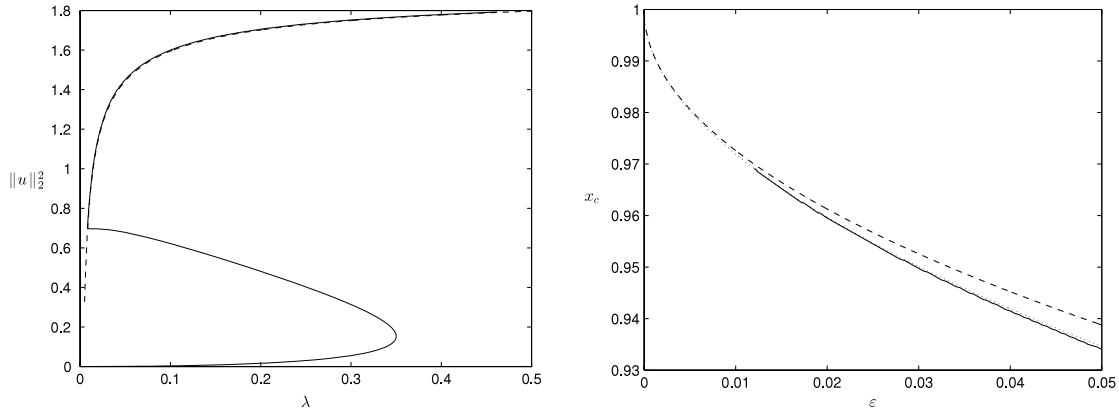

Fig. 9. Numerical verification of (4.11) and $p = 1/2$ for $m = 4$. The left panel displays the bifurcation diagram for $\varepsilon = 0.01$. The solid line represents the numerically obtained branches of solutions, while the dashed line is the asymptotic formula for the solution, as derived in (4.11). The right panel displays a comparison of the predictions for the equilibrium contact point $x_c = 1 - \sqrt{\varepsilon}\bar{x}_c$ with $\bar{x}_c$ given by (4.10), for fixed $\lambda = 10$ and a range of ε. The dashed line is the leading order expansion while the dotted is the three term.

where ξ_0 is a constant to be fixed in the matching procedure. The correction term at $\mathcal{O}(\varepsilon^{4p})$ solves

$$-w_{1\eta\eta\eta\eta} = \frac{\lambda_{0c}}{(1+w_0)^2}, \quad \eta \in (0,1); \qquad w_1(1) = w_{1\eta}(1) = 0 \tag{4.17}$$

and includes terms in $\log\eta$. The full solution is given by

$$w_1(\eta) = \left(2\beta_1 + \beta_2 + \frac{5}{486}\right)\eta^3 - \left(3\beta_1 + 2\beta_2 + \frac{5}{486}\right)\eta^2 + \beta_2\eta + \beta_1 + \left(\frac{16}{729}\eta^3 - \frac{2}{27}\eta^2 + \frac{2}{27}\eta - \frac{1}{54}\right) \times \Big(\log(3-2\eta) - \log\eta\Big),$$

where the constants β_1 and β_2 are arbitrary. In the transition layer near $x = x_c$, we define the local variables

$$u(x) = -1 + \varepsilon^{\nu} v(\xi), \quad \xi = \frac{x - x_c}{\varepsilon^q}, \tag{4.18}$$

and set the values $\nu = 1$ and $q = p + 1/2$. This transforms equation (3.13b) to

$$-v_{\xi\xi\xi\xi} = \lambda\varepsilon^{4p-1}\left(\frac{1}{v^2} - \frac{1}{v^m}\right), \qquad -\infty < \xi < \infty. \tag{4.19}$$

To make this equation independent of ε, we set $p = 1/4$. The far-field requirements are given by

$$\lim_{\xi\to-\infty} v(\xi) = 1 + \sigma(1);$$
$$-1 + \varepsilon v\left(\frac{\eta\,\bar{x}_c}{\varepsilon^{1/2}}\right) \sim w(\eta) \quad \text{as } \xi = \frac{\eta\,\bar{x}_c}{\varepsilon^{1/2}} \to \infty.$$

As in the Laplacian case, we will assume that the $\sigma(\varepsilon)$ term that appears in the far field condition as $\xi \to -\infty$ is of order ε^k with k large, or that it is small beyond all orders in ε, so that v approximately lies on the two-dimensional unstable manifold of the fixed point ($v = 1, v_\xi = 0, v_{\xi\xi} = 0, v_{\xi\xi\xi} = 0$) of the four-dimensional phase space associated to the above differential equation. We thus seek an expression for v that solves (4.19) to a given order in ε and satisfies the far-field conditions to that order as well. Eq. (4.19) may be integrated once to give

$$-v_{\xi\xi\xi}\,v_\xi + \frac{1}{2}\big(v_{\xi\xi}\big)^2 + \frac{\lambda}{v} - \frac{\lambda}{(m-1)v^{m-1}} = C, \tag{4.20}$$

where the constant of integration $C = \lambda\frac{m-2}{m-1}$ is determined by the value of the left-hand-side of (4.20) at the fixed point ($v = 1, v_\xi = 0, v_{\xi\xi} = 0, v_{\xi\xi\xi} = 0$). We set

$$v(\xi) = v_0(\xi) + \varepsilon^{1/2}v_1(\xi) + \varepsilon v_2(\xi) + \mathcal{O}(\varepsilon^{3/2}),$$

in (4.20) and solve the resulting equations at each order in half-integer powers of ε. Since the dominant term of $w(\eta)$ as $\eta \to 0$ is in η^2, the zeroth order solution $v_0(\xi)$ must behave like ξ^2 as $\xi \to \infty$. By substituting

$$v_0(\xi) = b_0\xi^2 + c_0\xi + d_0 + \eta_0\log\xi + \gamma_0\frac{\log\xi}{\xi^2} + \phi_0\frac{\log\xi}{\xi} + \frac{f_0}{\xi} + \frac{g_0}{\xi^2} + \mathcal{O}\left(\frac{\log\xi}{\xi^3}\right)$$

into the leading order equation and equating similar terms in ξ, we find

$$v_0(\xi) = b_0\xi^2 + c_0\xi + d_0 + \frac{\lambda}{6\,{b_0}^2}\log\xi + \frac{\lambda^2}{360\,{b_0}^5}\frac{\log\xi}{\xi^2} + \frac{\lambda\,c_0}{12\,{b_0}^3}\frac{1}{\xi} + \frac{\lambda\left(77\,\lambda - 540\,{c_0}^2b_0 + 180\,\delta_3{b_0}^2 + 360\,{b_0}^2d_0\right)}{21600\,{b_0}^5}\frac{1}{\xi^2} + \mathcal{O}\left(\frac{\log\xi}{\xi^3}\right),$$

where $2b_0^2 = C$ and $\delta_3 \equiv \delta(m-3)$ is equal to 1 if $m = 3$ and to 0 otherwise. Similar expressions for v_1 and v_2 are obtained and provided in the Appendix. We can then evaluate $-1+\varepsilon v(\xi)$ as $\xi \to \infty$, write the resulting expression as a function of $\eta = \sqrt{\varepsilon}\,\xi/\bar{x}_c$, and match with the expressions for $w_i(\eta)$ found for the boundary layer expansion. Note that $\bar{x}_c$ depends on λ_c (see (4.13c)), which itself depends on ε through Eq. (4.14b). At lowest order, we obtain

$$w_0(\eta) = -1 + b_0\eta^2\sqrt{\frac{\lambda_{0c}}{\lambda}} + a_1\eta^3\left(\frac{\lambda_{0c}}{\lambda}\right)^{3/4}$$

which must also be equal to $-1 + 3\eta^2 - 2\eta^3$. This fixes the values of b_0 and a_1 (the coefficient of ξ^3 in $v_1(\xi)$) to

$$b_0 = 3\sqrt{\frac{\lambda}{\lambda_{0c}}}, \qquad a_1 = -2\left(\frac{\lambda}{\lambda_{0c}}\right)^{3/4}.$$

With $2b_0^2 = C = \lambda(m-2)/(m-1)$, we obtain

$$\lambda_{0c} = \frac{18(m-1)}{(m-2)}. \tag{4.21}$$

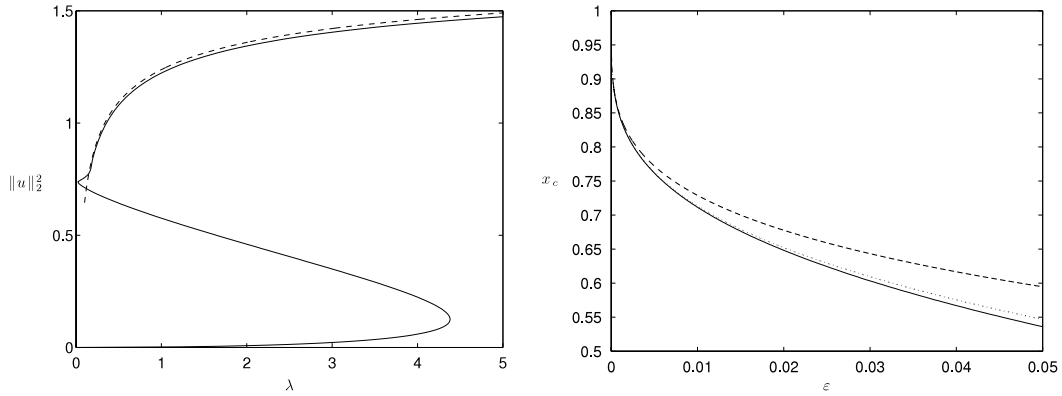

Fig. 10. Numerical verification of asymptotic calculations for the bi-Laplacian case and $m = 4$. The left panel displays the bifurcation diagram for $\varepsilon = 0.005$. The solid line represents the numerically obtained branches of solutions, while the dashed line is the asymptotic formula for the maximal solution, as derived in (4.26). The right panel displays a comparison of the one term (dashed line) and two term (dotted line) predictions for the equilibrium contact point $x_c = 1 - \varepsilon^{1/4}\bar{x}_c$ with $\bar{x}_c$ given by (4.25), for fixed $\lambda = 50$ and a range of ε.

Matching the expression for $w_{1/4}$ gives

$$a_2 = 0, \qquad c_0 = \xi_0 \left(\frac{\lambda}{\lambda_{0c}}\right)^{1/4} \qquad \lambda_{1c} = -\frac{2}{3}\xi_0 \lambda_{0c},$$

so that

$$\lambda_{1c} = -\frac{12(m-1)}{m-2}\xi_0. \tag{4.22}$$

The value of ξ_0 will be numerically estimated to be $\xi_0 \approx -3.77$ by imposing

$$v_0(0) = \min_{\xi \in \mathbb{R}} v_0(\xi). \tag{4.23}$$

This condition removes the translation invariance of (4.19) and therefore uniquely specifies the contact point. The expression for $w_{1/2}$ reads

$$w_{1/2}(\eta) = \frac{3}{2}\frac{\lambda_{2c}}{\lambda_{0c}}\eta^2 + \frac{1}{27}\lambda_{0c}\eta - \frac{1}{27}\lambda_{0c}\eta^2 - \frac{1}{108}\lambda_{0c} + \mathcal{O}(\eta^3)$$

and gives

$$\alpha_1 = -\frac{\lambda_{0c}}{108}, \qquad \alpha_2 = \frac{\lambda_{0c}}{27}, \qquad \lambda_{2c} = -\frac{\lambda_{0c}^2}{162}. \tag{4.24}$$

The w_1 term picks up the logarithmic singularity and reads

$$\begin{aligned} w_1(\eta) = {} & \left(\mathcal{O}(\eta^3) + \frac{2}{27}\lambda_{0c}\eta^2 - \frac{2}{27}\lambda_{0c}\eta + \frac{1}{54}\lambda_{0c}\right) \\ & \times \log\left(\eta\sqrt[4]{\frac{\lambda_{0c}}{\lambda}}\right) + \left(-\frac{3}{2}\frac{\lambda_{3c}}{\lambda_{0c}} + \frac{1}{12}\xi_0^2\right)\eta^3 \\ & + \left(-\frac{7}{81}\lambda_{0c} - c_1\sqrt[4]{\frac{\lambda_{0c}}{\lambda}} + \frac{3}{2}\frac{\lambda_{3c}}{\lambda_{0c}}\right)\eta^2 \\ & + \left(-\frac{1}{6}{\xi_0}^2 + c_1\sqrt[4]{\frac{\lambda_{0c}}{\lambda}}\right)\eta + d_0, \end{aligned}$$

leading to

$$d_0 = \beta_1 = \frac{7}{81}\lambda_{0c} + \frac{1}{12}{\xi_0}^2, \qquad \beta_2 = -\frac{1}{6}{\xi_0}^2 + \sqrt[4]{\frac{\lambda_{0c}}{\lambda}}\, c_1,$$

and

$$\lambda_{3c} = -\frac{28}{243}{\lambda_{0c}}^2 + \frac{1}{18}\lambda_{0c}{\xi_0}^2 - \frac{5}{729}\lambda_{0c} - 2/3\sqrt[4]{\frac{\lambda_{0c}}{\lambda}}\,\lambda_{0c}\, c_1.$$

Combining (4.22), (4.21), and (4.13c), the four term expansions for the contact points are

$$\begin{aligned} x_c = \pm\Bigg[1 - {} & \left[\frac{18(m-1)}{\lambda(m-2)}\right]^{1/4} \\ & \times \left(\varepsilon^{1/4} - \frac{\xi_0}{6}\varepsilon^{3/4} - \frac{\lambda_{0c}}{648}\varepsilon^{5/4}\log\varepsilon + \mathcal{O}(\varepsilon^{5/4})\right)\Bigg] \end{aligned}$$

where $\xi_0 \approx -3.77$.

To summarize, we expect the equilibrium solution u of (3.13b) to satisfy the following properties in the limit $\varepsilon \to 0$:

- $u(x) = -1 + \varepsilon + \sigma(\varepsilon^k)$, $k > 2$ in the interior region $x \in [0, x_c]$, with $x_c = 1 - \varepsilon^{1/4}\bar{x}_c$;
- $u(x) = -1 + \varepsilon\, v_0(\xi) + \varepsilon^{3/2} v_1(\xi) + \varepsilon^2 v_2(\xi) + \mathcal{O}(\varepsilon^{5/2})$ in the transition layer near x_c, with $\xi = \frac{x - x_c}{\varepsilon^{3/4}}$.
- $u(x) = -1 + 3\eta^2 - 2\eta^3 + \xi_0\,\eta\,(\eta - 1)^2\varepsilon^{1/2} + \mathcal{O}(\varepsilon\log\varepsilon)$ in the boundary layer $x \in (x_c, 1]$, with $\eta = \frac{x - x_c}{\varepsilon^{1/4}\bar{x}_c}$.

For comparison with the numerical bifurcation diagram, the squared L^2 norm of the composite asymptotic expansion is calculated to be

$$\begin{aligned} \|u\|_2^2 &= 2\left[\int_0^{1-\varepsilon^{1/4}\bar{x}_c} u(x)^2\,dx + \int_{1-\varepsilon^{1/4}\bar{x}_c}^1 u(x)^2\,dx\right] \\ &= 2\Big[(-1+\varepsilon+\sigma(\varepsilon))^2\Big(1 - \varepsilon^{1/4}\bar{x}_c\Big) \\ &\quad + \varepsilon^{1/4}\bar{x}_c\int_0^1 \left(w_0^2 + 2\varepsilon^{1/2}w_0 w_{1/4}\right)d\eta + \mathcal{O}(\varepsilon^{3/4})\Big] \end{aligned}$$

To simplify this expression, we calculate that

$$\int_0^1 w_0^2\,d\eta = \frac{13}{35}, \qquad \int_0^1 w_0 w_{1/4}\,d\eta = -\frac{11\xi_0}{210},$$

and apply the expansion

$$\bar{x}_c = \left[\frac{18(m-1)}{\lambda(m-2)}\right]^{1/4}\left(1 - \frac{\xi_0}{6}\varepsilon^{1/2} + \mathcal{O}(\varepsilon\log\varepsilon)\right), \tag{4.25}$$

which finally results in the value

$$\begin{aligned} &\|u(x;\varepsilon)\|_2^2 \\ &\quad = 2\left[1 - \frac{22}{35}\left(\frac{18(m-1)}{\lambda(m-2)}\right)^{1/4}\varepsilon^{1/4} + \mathcal{O}(\varepsilon^{3/4})\right]. \end{aligned} \tag{4.26}$$

This quantity is plotted (dashed curve) in the left panel of Fig. 10 as a function of λ for $m = 4$, and is in good agreement with the

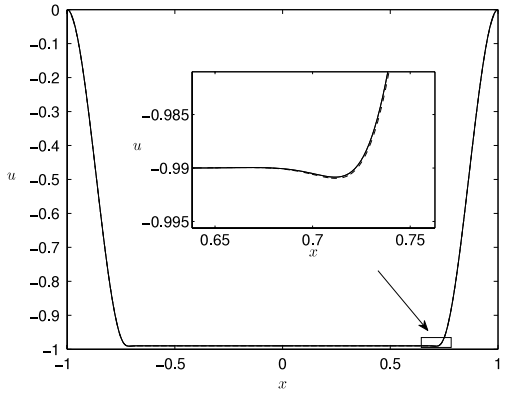

Fig. 11. Composite asymptotic expansion of equilibrium solutions to (3.13) for values $m = 4$, $\lambda = 50$, $\varepsilon = 0.01$. The solid line is the numerical solution and the dashed line is the composite asymptotic expansion.

numerically computed bifurcation diagram of Fig. 4. As before, the right panel of Fig. 10 is a numerical confirmation of the ε-scaling (with an exponent $p = 1/4$ in this case) of the width of the boundary layer.

4.3. Singular asymptotics and bistability

In this section, we briefly focus on another of the remarkable departures from the standard $\varepsilon = 0$ bifurcation diagram displayed by the regularized equations (3.13), namely the presence of bistability for a certain range of ε. Recall that the three characteristic bifurcation diagrams shown in Fig. 4 have the following features. For $\varepsilon \in (0, \varepsilon_c)$, the bifurcation diagrams of (3.13) have two fold points λ_* and λ^*, which results in bistable behavior for $\lambda_* < \lambda < \lambda^*$. At the critical value $\varepsilon = \varepsilon_c$, there is a single cubic fold point, while for $\varepsilon_c < \varepsilon$, there are no fold points and (3.13) has a unique solution for each λ.

In Fig. 12, the bifurcation diagrams of (3.13) are displayed for a range of $\varepsilon \in (0, \varepsilon_c)$ and $m = 4$. In each case, the fold point $\lambda_*(\varepsilon)$ is observed to depend quite sensitively on the parameter ε, while the principal fold point $\lambda^*(\varepsilon)$ exhibits smaller variations as ε increases. In essence, the regularizing term of the governing equations generates a regular perturbation to solutions of the $\varepsilon = 0$ problem whenever $1 + u = \mathcal{O}(1)$, and a singular perturbation to solutions of the $\varepsilon = 0$ problems whenever $u + 1 \simeq \varepsilon$. In each of the cases represented in Fig. 12, the two fold points are empirically seen to be increasing functions of ε, with $\lambda_*(\varepsilon)$ increasing faster than $\lambda^*(\varepsilon)$. We therefore expect the two fold points to eventually merge at some critical ε_c, where the condition

$$\lambda_*(\varepsilon_c) = \lambda^*(\varepsilon_c) \tag{4.27}$$

is satisfied. The bistable features of the regularized system are interesting as they give the device the capacity to switch robustly between equilibrium states of large and small L^2 norm. The relative magnitude of the switching voltage required to transition the device between these two states is given, for $\varepsilon < \varepsilon_c$, by the quantity $\lambda^*(\varepsilon) - \lambda_*(\varepsilon)$.

It is therefore desirable to obtain explicit formulae for $\lambda_*(\varepsilon)$ and $\lambda^*(\varepsilon)$ so that the critical parameter ε_c may be estimated from the condition (4.27) and the bistable nature of the regularized system understood. In a forthcoming paper [44], a detailed singular perturbation analysis is employed to accurately locate these fold points. The main results are explicit expansions of form

$$\lambda^*(\varepsilon) \sim \lambda_0^* + \varepsilon^{m-2}\lambda_1^* + \mathcal{O}(\varepsilon^{2(m-2)}), \tag{4.28a}$$

for the principal fold point in the Laplacian or bi-Laplacian case. The scaling of the second fold point is quite different for the second and fourth order problems, namely

$$\begin{aligned} &\lambda_*(\varepsilon) \sim \lambda_{*0}\varepsilon + \lambda_{*1}\varepsilon^2 \log\varepsilon + \lambda_{*2}\varepsilon^2 + \cdots && \text{(Laplacian)} \\ &\lambda_*(\varepsilon) \sim \lambda_{*0}\varepsilon^{3/2} + \lambda_{*1}\varepsilon^2 + \cdots && \text{(bi-Laplacian)} \end{aligned} \tag{4.28b}$$

In the above formulations, closed form expressions for the coefficients λ_{*i} and λ_i^* are established in [44].

5. Discussion

In this work we have proposed and analyzed a formulation for regularization of touchdown in MEMS capacitors. These considerations have resulted in a new family of models whose solutions remain globally bounded in time for all parameter regimes, followed by equilibration to new steady states. Interestingly, the presence of these new stable equilibria results in bistable behavior for a range of parameter values. This may be useful in practical applications since bistable systems can be used to create robust switches. We have described how equilibrium solutions depend on the parameters λ and ε in terms of bifurcation diagrams, for both the Laplacian and the bi-Laplacian cases. Using asymptotic analysis, we have also given a complete characterization of the scaling properties of the upper branch of equilibrium solutions, which correspond to attracting post-touchdown configurations of the regularized equations.

There are several avenues of future exploration emanating from this study. The method of regularization used in the present work is a first attempt at understanding the behavior of MEMS after touchdown. It is natural to ask whether this bistability feature is generic to a larger family of regularized models.

An interesting problem is the characterization of the intermediate dynamics between the initial regularized touchdown event

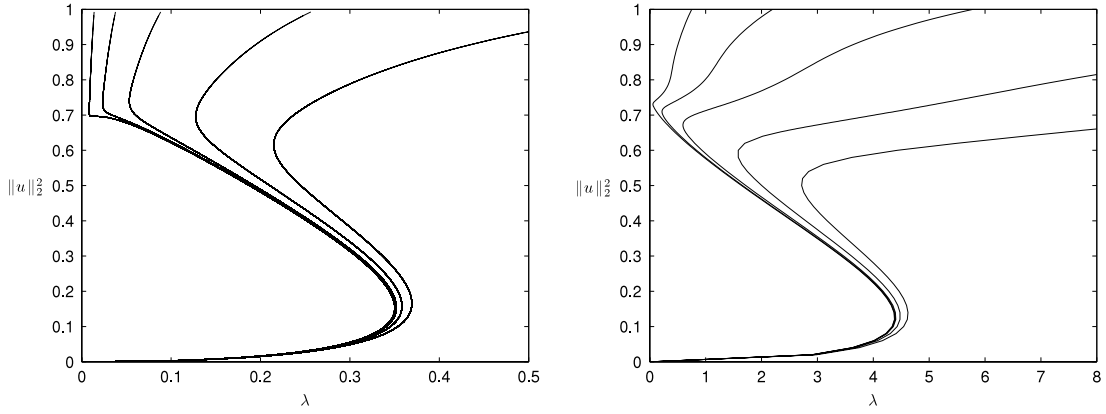

Fig. 12. Numerically obtained bifurcation diagrams of (3.13) for $\varepsilon = 0.01, 0.025, 0.05, 0.1, 0.15$ (from left to right) and $m = 4$. Left panel: Laplacian case (3.13a); right panel: bi-Laplacian case (3.13b).

and the equilibration to the post touchdown states. As is typical with such obstacle type regularizations, the equations (2.12) give rise to a free boundary problem for the extent of the touchdown region, which is amenable to analysis. In a forthcoming paper [43], we describe the dynamic evolution of the periphery of the growing post-touchdown region, in both one and two spatial dimensions.

Acknowledgments

K.G. acknowledges support from National Science Foundation award DMS-0807423. A.E.L acknowledges support from the Carnegie Trust for the Universities of Scotland. A.E.L and J.L. completed the manuscript during a stay at the Henri Poincaré Institute in July 2013 and thank them for their hospitality.

Appendix. Expressions for v_1 and v_2

We give below the expressions for $v_1(\xi)$ and $v_2(\xi)$ such that $v = v_0 + \varepsilon^{1/2} v_1 + \varepsilon v_2 + \mathcal{O}(\varepsilon^{3/2})$ solves (4.20) to order $\varepsilon^{1/2}$ and ε respectively.

$$\begin{aligned} v_1(x) &= a_1\xi^3 + \frac{3a_1c_0}{2b_0}\xi^2 + c_1\xi + d_1 + \frac{\lambda\, c_0 a_1}{2\,{b_0}^4}\log(\xi) \\ &\quad + \frac{\lambda\, a_1}{{b_0}^3}\xi\log(\xi) + \frac{\lambda^2 a_1}{24\,{b_0}^6}\frac{\log(\xi)}{\xi} + \gamma_1\frac{\log(\xi)}{\xi^2} \\ &\quad - \frac{\lambda\left(-36\,{c_0}^2 a_1 b_0 + 72\,d_0 a_1 {b_0}^2 - 24\,c_1{b_0}^3 - 25\,\lambda\, a_1 + 36\,\delta_3 a_1 {b_0}^2\right)}{288\,{b_0}^6\xi} \\ &\quad + \frac{g_1}{\xi^2} + \mathcal{O}\left(\frac{\log(\xi)}{\xi^3}\right), \end{aligned}$$

and

$$\begin{aligned} v_2(\xi) &= a_2\xi^3 + b_2\xi^2 + c_2\xi + d_2 + \kappa_2(\log(\xi))^2 \\ &\quad + \eta_3\log(\xi) + \eta_4\,\xi\log(\xi) + \eta_5\,\xi^2\log(\xi) \\ &\quad + \phi_2\frac{\log(\xi)}{\xi} + \gamma_2\frac{\log(\xi)}{\xi^2} + \frac{f_2}{\xi} + \frac{g_2}{\xi^2} + \mathcal{O}\left(\frac{\log(\xi)}{\xi^3}\right), \end{aligned}$$

where

$$\eta_3 = \lambda\,\frac{\left(-18\,\delta_3 {a_1}^2 {b_0}^2 + 16\,\lambda\,{a_1}^2 + 9\,a_2 c_0 {b_0}^3 + 9\,{a_1}^2 {c_0}^2 b_0 - 36\,{a_1}^2 {b_0}^2 d_0 + 9\,a_1 c_1 {b_0}^3\right)}{18\,{b_0}^7},$$

$$\eta_4 = \frac{6\,\lambda\, c_0 {a_1}^2 + 4\,\lambda\, a_2 {b_0}^2}{4\,{b_0}^5}, \qquad \eta_5 = \frac{3\lambda\,{a_1}^2}{2\,{b_0}^4}, \qquad \kappa_2 = \frac{\lambda^2 {a_1}^2}{12\,{b_0}^7},$$

$$b_2 = -\frac{14\,\lambda\,{a_1}^2 - 12\,a_2 c_0 {b_0}^3 + 9\,{a_1}^2 {c_0}^2 b_0 - 12\,a_1 c_1 {b_0}^3}{8\,{b_0}^4},$$

$$\phi_2 = -\frac{-4\,\lambda^2 a_2 {b_0}^2 + 7\,\lambda^2 c_0 {a_1}^2 + 720\,a_1\gamma_1 {b_0}^7}{96\,{b_0}^8},$$

$$\begin{aligned} f_2 &= \frac{\lambda\, c_0\left(36\,{c_0}^2 b_0 + 341\,\lambda - 72\,{b_0}^2 d_0 - 36\,\delta_3 {b_0}^2\right){a_1}^2}{1152\,{b_0}^8} \\ &\quad - \frac{\left(\lambda\, c_0 c_1 + \lambda\, d_1 b_0 + 60\,g_1 {b_0}^4 + 48\,\gamma_1 {b_0}^4\right)a_1}{8\,{b_0}^5} \\ &\quad + \frac{\lambda\left(-72\,{b_0}^2 d_0 + 25\,\lambda + 36\,{c_0}^2 b_0 - 36\,\delta_3 {b_0}^2\right)a_2}{288\,{b_0}^6} + \frac{\lambda\, c_2}{12\,{b_0}^3}. \end{aligned}$$

References

[1] Anubhav Arora, Mark R. Prausnitz, Samir Mitragotri, Micro-scale devices for transdermal drug delivery, Int. J. Pharm. 364 (2) (2008) 227–236.
[2] Nan-Chyuan Tsai, Chung-Yang Sue, Review of MEMS-based drug delivery and dosing systems, Sensors Actuators A 134 (2) (2007) 555–564.
[3] Brian D. Iverson, Suresh V. Garimella, Recent advances in microscale pumping technologies: a review and evaluation, Microfluid. Nanofluidics 5 (2) (2008) 145–174.
[4] N. Doble, D.R. Williams, The application of MEMS technology for adaptive optics in vision science, IEEE J. Sel. Top. Quantum Electron. 10 (3) (2004) 629–635.
[5] B. Watson, J. Friend, L. Yeo, Piezoelectric ultrasonic micro/milli-scale actuators, Sensors Actuators A 152 (2009) 219–233.
[6] N. Ghoussoub, Y. Guo, Estimates for the quenching time of a parabolic equation modeling electrostatic MEMS, Methods Appl. Anal. 15 (3) (2008) 361–376.
[7] N. Ghoussoub, Y. Guo, On the partial differential equations of electrostatic MEMS devices III: dynamic case, Nonlinear Differ. Equ. Appl. 15 (2008) 115–145.
[8] Y. Guo, Z. Pan, M. J. Ward, Touchdown and pull-in voltage behaviour of a MEMS device with varying dielectric properties, SIAM J. Appl. Math. 66 (1) (2005) 309–338.
[9] N. I. Kavallaris, A. A. Lacey, C. V. Nikolopoulos, D. E. Tzanetis, A hyperbolic non-local problem modelling MEMS technology, Rocky Mountain J. Math 41 (2) (2011) 349–630.
[10] J. A. Pelesko, Mathematical modeling of electrostatic MEMS with tailored dielectric properties, SIAM J. Appl. Math. 62 (3) (2002) 888–908.
[11] N. D. Brubaker, J. A. Pelesko, Non-linear effects on canonical MEMS models, European J. Appl. Math. 22 (5) (2011) 455–470.
[12] A. E. Lindsay, J. Lega, F.-J. Sayas, The quenching set of a MEMS capacitor in two-dimensional geometries, J. Nonlinear Sci. 23 (5) (2013) 807–834.
[13] A. E. Lindsay, J. Lega, Multiple quenching solutions of a fourth order parabolic PDE with a singular nonlinearity modelling a MEMS capacitor, SIAM J. Appl. Math. 72 (3) (2012) 935–958.
[14] F. H. Lin, Y. Yang, Nonlinear non-local elliptic equation modeling electrostatic actuation, Proc. R. Soc. A 463 (2007) 1323–1337.
[15] Y. Guo, Dynamical solutions of singular wave equations modeling electrostatic MEMS, SIAM J. Appl. Dyn. Syst. 9 (2010) 1135–1163.
[16] Ph. Laurençot, C. Walker, A fourth-order model for MEMS with clamped boundary conditions, http://arxiv.org/abs/1304.2296.
[17] R. C. Batra, M. Porfiri, D. Spinello, Effects of van der Waals force and thermal stresses on pull-in instability of clamped rectangular microplates, Sensors 8 (2008) 1048–1069.
[18] J-G. Guo, Y-P. Zhao, Influence of van der Waals and Casimir forces on electrostatic torsional actuators, J. Microelectromech. Syst. 13 (6) (2004) 1027–1035.
[19] B. Lai, On the partial differential equations of electrostatic MEMS devices with effects of Casimir force, Ann. Henri Poincaré (2014) http://dx.doi.org/10.1007/s00023-014-0322-8.
[20] A. J. Bernoff, T. P. Witelski, Stability and dynamics of self-similarity in evolution equations, J. Engrg. Math. 66 (1–3) (2010) 11–31.
[21] A. J. Bernoff, A. L. Bertozzi, T. P. Witelski, Axisymmetric surface diffusion: dynamics and stability of self-similar pinch-off, J. Stat. Phys. 93 (1998) 725–776.
[22] A. J. Bernoff, T. P. Witelski, Stability of self-similar solutions for van der Waals driven thin film rupture, Phys. Fluids 11 (9) (1999).
[23] J. A. Pelesko, D. H. Bernstein, Modeling MEMS and NEMS, Chapman Hall and CRC Press, 2002.
[24] N. Ghoussoub, Y. Guo, On the partial differential equations of electrostatic MEMS devices: stationary case, SIAM J. Math. Anal. 38 (5) (2007) 1423–1449.
[25] P. Esposito, N. Ghoussoub, Y. Guo, Mathematical Analysis of Partial Differential Equations Modeling Electrostatic MEMS, in: Courant Lecture Notes, vol. 20, 2010.
[26] G. Flores, G. Mercado, J. A. Pelesko, N. Smyth, Analysis of the dynamics and touchdown in a model of electrostatic MEMS, SIAM J. Appl. Math. 67 (2) (2007) 434–446.
[27] Y. Guo, On the partial differential equations of electrostatic MEMS devices III: refined touchdown behavior, J. Differential Equations 244 (2008) 2277–2309.
[28] A. E. Lindsay, M. J. Ward, Asymptotics of some nonlinear eigenvalue problems for a MEMS capacitor: Part I: fold point asymptotics, Methods Appl. Anal. 15 (3) (2008) 297–325.
[29] Z. Guo, B. Lai, D. Ye, Revisiting the biharmonic equation modeling electrostatic actuation in lower dimensions, Proc. Amer. Math. Soc. 142 (2014) 2027–2034.
[30] A. E. Lindsay, An asymptotic study of blow up multiplicity in fourth order parabolic partial differential equations, Discrete Contin. Dyn. Syst. Ser. B 19 (1) (2014) 189–215.
[31] Ph. Laurençot, C. Walker, A stationary free boundary problem modelling electrostatic MEMS, Archive for Rational Mechanics and Analysis 207 (2013) 139–158.
[32] J. Escher, Ph. Laurençot, C. Walker, Dynamics of a free boundary problem with curvature modeling electrostatic MEMS, Trans. Amer. Math. (2014) http://arxiv.org/abs/1302.6026 (in press).
[33] J. Escher, Ph. Laurençot, C. Walker, Finite time singularity in a free boundary problem modeling MEMS, C. R. Acad. Sci. Paris Sér. I Math. 351 (2013) 807–812.
[34] M. Kohlmann, A new model for electrostatic MEMS with two free boundaries, J. Math. Anal. Appl. 408 (2) (2013) 513–524.
[35] Ph. Laurençot, C. Walker, A free boundary problem modeling electrostatic MEMS I. Linear bending effects, Math. Ann. (2014) http://dx.doi.org/10.1007/s00208-014-1032-8 (in press).
[36] Ph. Laurençot, C. Walker, A free boundary problem modeling electrostatic MEMS II. Non-linear bending effects, Math. Models Methods Appl. Sci. (2014) http://dx.doi.org/10.1142/S0218202514500298 (in press).
[37] G. Flores, Dynamics of a damped wave equation arising from MEMS, SIAM J. Appl. Math (2014) (in press).
[38] J.-S. Guo, B.-C. Huang, Hyperbolic quenching problem with damping in the micro-electro mechanical system device, Discrete Contin. Dyn. Syst. Ser. B 19 (2) (2014) 419–434.
[39] N. Kikuchi, J. T. Oden, Contact Problems in Elasticity: A Study of Variational Inequalities and Finite Element Methods, SIAM, 1988.
[40] J-L. Lions, Quelques Méthodes de Résolution des Problemes Aux Limites Non Linéaires, vol. 76, Dunod, Paris, 1969.
[41] R. Scholz, Numerical solution of the obstacle problem by the penalty method, Numer. Math. 49 (2–3) (1986) 255–268.
[42] A. L. Bertozzi, G. Grün, T. P. Witelski, Dewetting films: bifurcations and concentrations, Nonlinearity 14 (2001) 1569–1592.
[43] A.E. Lindsay, J. Lega, K.B. Glasner, Regularized model of post-touchdown configurations in electrostatic MEMS: Interface Dynamics, preprint.
[44] A.E. Lindsay, Regularized model of post-touchdown configurations in electrostatic MEMS: bistability properties, preprint.
[45] A. E. Lindsay, M. J. Ward, Asymptotics of some nonlinear eigenvalue problems for a MEMS capacitor: Part II: singular asymptotics, European. J. Appl. Math. 22 (2011) 83–123.